Equilibrium scour depth prediction around cylindrical structures

N. S. Tavouktsoglou[1], J. M. Harris[2], R. R. Simons[3] & R. J. S. Whitehouse[4]

[1]Engineering Doctorate candidate, Dept. of Civil, Environmental and Geomatic Engineering, University College London, London, WC1E 6BT, UK, (corresponding author). E-mail: n.tavouktsoglou@ucl.ac.uk

[2]Technical Director, Coasts and Estuaries, HR Wallingford, Wallingford, OX10 8BA, UK. E-mail: j.harris@hrwallingford.com

[3]Professor of Fluid Mechanics and Coastal Engineering, Dept. of Civil, Environmental and Geomatic Engineering, University College London, London, WC1E 6BT, UK. E-mail: r.r.simons@ucl.ac.uk

[4]Technical Director, Coasts and Estuaries, HR Wallingford, Wallingford, OX10 8BA, UK. E-mail: r.whitehouse@hrwallingford.com

Abstract

Offshore Gravity Base Foundations (GBFs) are often designed with complex geometries. Such structures interact with the local hydrodynamics, creating an adverse pressure gradient which is responsible for flow and scour phenomena including the bed shear stress amplification. In this study a method is presented for predicting clearwater scour around cylindrical structures with non-uniform geometries under the forcing of a unidirectional current. The interaction of the flow field with the sediment around these complex structures is described in terms of non-dimensional parameters that characterize the similitude of water-sediment movement. The paper presents insights to the influence the streamwise depth-averaged Euler number has on the equilibrium scour around uniform and non-uniform cylindrical structures. Here the Euler number is based on the depth-averaged streamwise pressure gradient (calculated using potential flow theory), the mean flow velocity and the fluid density.

Following a dimensional analysis, the controlling parameters were found to be the Euler number, pile Reynolds number, Froude number, sediment mobility number and the non-dimensional flow depth. Based on this finding a new scour prediction equation was developed. This new method shows good agreement with the database of scour depths acquired in this study ($R^2 = 0.91$). Measurements of the equilibrium scour depth around non-

uniform cylindrical structures are used to show the importance of the Euler number on the scour process. Finally, the importance of the remaining non-dimensional quantities with respect to scour is also investigated in this study.

Introduction

Research into scour around offshore foundations has mainly been focused on the impacts different hydrodynamic conditions have on the bed when they interact with a monopile. A systematic review is given by Whitehouse (1998) and Sumer and Fredsøe (2002). While a considerable amount of research has been conducted for the fluid-structure-soil interaction around monopiles, extensive research for more complex structures such as Gravity Base Foundations (GBFs) has not been conducted, although the resulting scour has been analysed by Whitehouse et al. (2011).

Interest in renewable energy on a global level has enabled the offshore wind industry to plan and construct a large number of offshore wind farms in shallow waters (10 to 30m). Due to the increasing demand for offshore wind energy, wind farm locations are being planned for greater water depths (30 to 60m). These locations are characterized by hydraulic conditions that are similar to those faced by offshore oil platforms where wave conditions may be more energetic, but the influence of waves on scour may be less pronounced due to the increased water depth, whilst tidal currents may be more dominant. This is because the bed orbital velocities at greater water depths will be smaller than those in shallower waters for an identical wave, which may lead to less wave generated scour and backfilling compared to the shallow water case. In these locations GBFs may become a more cost competitive support structure for wind turbines relative to monopiles foundation because:

- construction material (i.e. concrete) is readily available and at a lower cost compared to steel;
- GBFs tend to be stiffer structures which may lead to advantages with respect to blade passing and wave excitation frequencies;
- GBFs that are floating towable structures can lead to the faster installation of the foundation; and,
- GBFs can be fabricated near the installation site, thus decreasing the transportation costs.

There has been a limited amount of research into the scour potential of non-uniform cylindrical structures. One of the first studies on scour around composite structural geometries is reported by Chabert and Engeldinger (1956), who examined the influence of a larger diameter foundation footing has on scour; their results showed that the equilibrium scour depth was significantly reduced when the footing was below the original bed level. The first investigation into scour around a GBF is given by Teramoto et al. (1973) who concluded that the controlling factor of scour for sit-on-bottom structures is the structure's height, and they derived a scour prediction formula for the time development of scour for rectangular submerged structures. The effect conical GBF structures have on scour was investigated by Khalfin (1983). Khalfin concluded that the scour formation and depth were fundamentally different for cylindrical and conical GBFs, and also derived a prediction formula for the determination of the equilibrium scour under the forcing of currents. Hoffmans and Verheij (1997) modified Khalfin's formula to extend its applicability for rectangular structures and proposed the use of an equivalent diameter of the structure in order to use the formula for more complex geometries. Subsequently Bos et al. (2002) conducted a study on scour around large-scale submerged offshore structures subjected to the combined effect of wind waves and currents. The study agreed with the findings of Teramoto et al. (1973) and developed an equilibrium scour prediction formula for rectangular submerged GBFs for situations with low U/U_c, i.e. low sediment mobility. In addition to this, some research has been conducted in the context of scour around complex pier shaped foundations in rivers. Examples of such studies are Jones et al. (1992), Parola et al. (1996) and Melville and Raudkivi (1996) who investigated the effect of the bottom footing of a pier on scour, and proposed different empirical equations to obtain an equivalent diameter length scale for non-dimensionalising the equilibrium scour depth. These studies reveal important information about the effect of different parameters on scour development around GBFs, but they also show that there is not a unified approach for determining the equilibrium scour for different types of structures (submerged-emerged, cylindrical and complex geometries).

This paper presents a method for predicting the equilibrium scour depth around uniform and non-uniform cylindrical structures. The method was derived using newly generated physical model results and a wide range of equilibrium scour depth data from previously published studies. The method is based on a functional relationship between the equilibrium scour depth and non-dimensional quantities that arise from a similitude analysis. These variables include the non-dimensional flow depth, sediment mobility ratio, pile Reynolds number, Froude number and Euler number. Here the Euler number is defined using the depth-averaged pressure gradient, which is a physical quantity that has never been used in the past to describe the scour process.

The structure of this paper is as follows. Firstly, the similitude of the non-dimensional quantities that describe the scour processes are presented along with the formulation of the pressure gradient. Then, the details of the equilibrium scour database and the physical modelling tests are presented. The paper then presents the derivation of the scour prediction formula based on the Buckingham π theorem. The results and the importance of each of the non-dimensional parameters on the equilibrium scour are then discussed.

Similitude of scour at complex geometries

The flow-structure-bed interaction around both complex and uniform cylinders can be described in terms of non-dimensionalised parameters. For a steady-state flow with an isotropic, homogeneous Newtonian fluid over a flat bed comprised of cohesioneless sediment the most important variables that describe the interaction are:

$$S = f(\rho, \mu, \Delta p, D, h, g, U, U_c) \tag{1}$$

Here ρ is the fluid density; μ the dynamic viscosity of the fluid; Δp the change in the local pressure in the streamwise direction induced by the structure; D is the diameter of the structure in the case of a monopile, and the diameter of the base in the case of a complex structure as suggested by Yeow and Cheng (2003); h is the flow depth; g the gravitational acceleration; S is the equilibrium scour depth; U the depth-averaged flow velocity and U_c is the critical depth-averaged velocity for bed sediment movement, which can be calculated using the Soulsby (1997) method:

$$U_c = 7\left(\frac{h}{d_{50}}\right)^{\frac{1}{7}} [g(s-1)d_{50}f(D_*)]^{0.5} \tag{2}$$

with

$$f(D_*) = \frac{0.30}{1+1.2D_*} + 0.055[1 - \exp(-0.02D_*)] \tag{3}$$

$$D_* = \left[\frac{g(s-1)}{\nu^2}\right]^{\frac{1}{3}} d_{50} \tag{4}$$

Further, d_{50} is the median sediment diameter, s is the ratio of sediment grain density in water, and ν kinematic viscosity of water.

By adopting a polar coordinate system, Δp in equation (1) can then be represented in terms of the pressure gradient by taking the derivative in the angular direction (φ) (see Figure 1 for definition sketch); this can be calculated using potential flow theory. This yields:

$$S = f\left(\rho, \mu, \frac{dp}{d\varphi}, D, h, g, U, U_c\right) \tag{5}$$

By applying the Buckingham π theorem with normalising variables ρ, D and U the following dependence is obtained for the non-dimensional scour depth S/D:

$$\frac{S}{D} = f\left(\frac{\frac{dp}{d\varphi}}{U^2\rho}, \frac{\mathrm{U}}{\sqrt{gh}}, \frac{U}{U_c}, \frac{UD\rho}{\mu}, \frac{h}{D}\right) \tag{6}$$

This expression is equivalent to:

$$\frac{S}{D} = f\left(Eu, Fr, \frac{U}{U_c}, Re_D, \frac{h}{D}\right) \tag{7}$$

This expression suggests that the pile Reynolds number ($Re_D = UD/\nu$) is the form of Re that best characterises the effect on the scour process. Indeed this is verified when considering that the flow conditions in most experimental and prototype conditions are fully developed, thus making viscous effects negligible for a channel $Re = \frac{Uh}{\nu} > 10^4$ (Hughes, 1993). In addition, the critical grain Reynolds number is also considered implicitly in expression (7) as $U_c \propto \sqrt{\theta_c} \propto Re_*$ which implies that the effects of hydrodynamically rough and smooth flows are also considered through the Shields parameter θ_c.

Both Re_D and Eu are of importance in the scour process. The pile Reynolds number controls two important aspects of the flow structure interaction. Firstly, the separation point of the flow along the perimeter of a cylinder shifts towards the lee of the pile for an increasing Re_D (Achenbach, 1968). This results in a narrower wake, which translates into a delay in the separation of the boundary layer, a weaker horseshoe vortex at the upstream face of the structure (Roulund et al., 2005) and a smaller equilibrium non-dimensional scour depth. Secondly, the frequency of the lee wake vortices is altered. For cylinders in the same approach flow, the vortex shedding frequency process will be influenced by any change in the structures' diameter (i.e. change in the pile Reynolds number) (Sarpkaya, 2010). This change in Re_D will result in changes in the size of the vortices and their frequency (Melville, 2008). The importance of turbulent structures at the lee of structures with respect to scour was confirmed through a series of experiments by Ettema et al., 2006. In the study the vorticity and shedding frequency around cylinders were measured, showing that the small cylinders produce twice as much vorticity compared to the larger cylinders. According to Ettema et al., (2006) this difference is one of the mechanisms that contribute towards the general tendency of finding smaller non-dimensional scour depths in prototype conditions compared to experimental. This can partially explain the discrepancies between small scale laboratory experiments and prototype scour measurements, the latter tending to have relatively small non-dimensional scour depths (Ettema et al., 2006) whereas prototype observations of scour in the field with live-bed conditions can be large (i.e. scour depth around 1.8D; Harris and Whitehouse, 2015).

Expression (7) shows that both the pile Reynolds number and the Euler number are of particular importance when attempting to describe the processes involved in scour around uniform and complex structures. To the authors' knowledge this form of the Euler number has not previously been used to describe the scour process. In the context of scour Eu has only been discussed in Ettema et al. (2006) who argues that, for uniform cylinders, U^2/gD is a form of the Euler number as it emerges from the Euler equation when applied to a water surface across an eddy. This is equivalent to describing the lee wake vorticity intensity. The formulation shown in (7) differs from most existing scour prediction formulae (e.g. Khalfin, 1983, for shallow foundations; Breusers et al., 1977; and Johnson, 1992, for deep foundations) that are based only on:

$$\frac{S}{D} = f\left(Fr, \frac{U}{U_c}, \frac{h}{D}\right) \tag{8}$$

As mentioned previously the Euler number is the non-dimensional form of the adverse pressure gradient induced by the flow-structure interaction. This pressure gradient is responsible for the formation of the horseshoe vortex and explains the flow structure interaction outside the pile wall boundary layer and outside the lee wake region where the viscous effects are negligible. By approximating that the flow boundary layer of the structure is fully developed the pressure at the face of the structure can be determined by applying Prandtl's boundary layer theory with the familiar Bernoulli equation in polar coordinates:

$$\frac{u_\varphi^2 + u_r^2}{2g} + \frac{p}{\gamma} + z = C \tag{9}$$

where:

γ is the specific gravity of water, p is the pressure, u_φ is the tangential component of the velocity in polar coordinates with its origin at the centre of the structure, u_r is the radial component of the velocity in polar coordinates with its origin at the centre of the structure, z is the height above the initial bed, and C is a constant. When combined with the equations for the velocity in the tangential and radial direction this yields equation (10):

$$z + \frac{p}{\gamma} + \frac{1}{2g}u(z)^2\left(\frac{\left(\frac{D}{2}\right)^4}{r^4} - \frac{2\left(\frac{D}{2}\right)^2}{r^2}\cos(2\varphi) + 1\right) = C \tag{10}$$

And by differentiating with respect to φ:

$$\frac{dp}{d\varphi} = -2\rho u(z)^2\left(\frac{\left(\frac{D(z)}{2}\right)^2}{r^2}\right)\sin(2\varphi) \tag{11}$$

where:

z is the vertical distance from the bed, ρ is the density of water, φ is the angle relative to the approach flow direction, $D(z)$ is the diameter of the structure as a function of the vertical distance from the bed for complex geometries, $\frac{dp}{d\varphi}$ is the pressure gradient at any given location around the structure, r is the distance from the pier centre where the pressure gradient is evaluated, and $u(z)$ is the approach velocity at any given height "z" above the initial bed.

An estimate of the effect the pressure gradient has on the bed can then be determined by calculating the depth-averaged pressure gradient ($\langle dp/d\varphi \rangle$) which leads to equation (12).

$$\langle \frac{dp}{d\varphi} \rangle = \frac{1}{h} \int_0^h \left(-2\rho u(z)^2 \left(\frac{\left(\frac{D(z)}{2}\right)^2}{r^2} \right) \sin(2\varphi) \right) dz \qquad (12)$$

In equation (12) the integration assumes that there is no energy transfer between the fluid layers in the water column and the velocity profile can be approximated by the equations of the hydrodynamically rough velocity profile given in Einstein (1950) (i.e. equations 13 and 14) and the Nikuradse roughness (equation 15):

$$\frac{u(z)}{U_f} = 8.6 + 2.5 \ln\left(\frac{z}{k_s}\right) \qquad (13)$$

where:

$$U_f = \frac{U}{6.0 + 2.5 \ln\left(\frac{h}{k_s}\right)} \qquad (14)$$

$$k_s = 2.5\, d_{50} \qquad (15)$$

d_{50} is the median sediment size; k_s is the roughness length-scale; h is the water depth and U_f is the friction velocity based on the depth-averaged velocity and median sediment diameter.

The maximum depth-averaged pressure gradient can then be determined by integrating throughout the water column at the point where the maximum tangential pressure gradient is expected (i.e. $\varphi = \pi/4\ and\ r = D_{base}/2$) which leads to expression (16).

$$\langle \frac{dp}{d\varphi} \rangle_{max} = \left| \frac{1}{h} \int_0^h \left(-2\rho u(z)^2 \left(\frac{D(z)}{D_{base}} \right) \right) dz \right| \qquad (16)$$

where D_{base} is the diameter of the base of the structure (Figure 1a).Equation (16) implies that for the same hydrodynamic conditions the structure that has a non-uniform structure geometry such as a conical base structure of increasing diameter towards the bed will have a smaller depth-averaged pressure gradient compared to a monopile. This in turn would result in a smaller downflow on the face of the structure, a reduced amplification of the bed shear stress and thus, smaller scour depths. This statement is verified by Tavouktsoglou et al. (2015) who measured the amplification of the bed shear stress for the same flow conditions and structures for which the pressure gradient distribution is calculated in Figure 2. The pressure gradients were calculated for two of the small scale structures listed in Figure 3 and for a mean flow velocity of 0.39 m/s and a water depth of 0.165 m. They found that there is a significant increase in the amplification of the bed shear stress between a conical base structure and a monopile, which agrees qualitatively with the pressure gradient profiles depicted in Figure 2. Similarly, equation (16) suggests that different vertical distributions of the flow profile also have an effect on the pressure gradient and thus on the scour potential for a given situation. Figure 1 (a) shows a structure that has been subjected to two different flow conditions u_1 and u_2 with different depth profiles but the same overall flow flux (i.e. same depth-averaged velocity). Applying equation (16) to these two cases, the profile u_2 produces a smaller depth-averaged pressure gradient compared to that in $u_1$as smaller velocities are interacting with the widest portion of the structure. This phenomenon is of particular interest in practice when considering flows in locations where large lateral wind loads are expected such as the locations where offshore wind farms are situated. In these locations the wind load effectively produces a wind driven shear flow on top of the existing logarithmic flow creating a flow profile similar to that of u_2 in Figure 1 (a) (Davies and Lawrence, 1994).

Based on equations (6) and (16) the non-dimensional form of the depth-averaged pressure gradient can now be defined as the depth-averaged Euler number, which can be written as follows:

$$\langle Eu \rangle = \frac{\langle \frac{dp}{d\varphi} \rangle_{max}}{U^2 \rho} \tag{17}$$

For the simpler case of a logarithmic flow profile interacting with a uniform cylinder the Euler number can conservatively be assumed to take a value of 2 (Tavouktsoglou et al., 2016). For all other conditions designers are recommended to:

- establish a functional relationship that describes the vertical distribution of the streamwise flow velocity $\big(u(z)\big)$;
- create a function that describes the diameter of the non-cylindrical structure $\big(D(z)\big)$ as a function of the distance from the bed (z); and,
- calculate the depth-averaged pressure gradient though the integration of equation (16) or by evaluating equation (16) at a minimum of 50 points throughout the water column and substituting in expression (17). This process can be automated in a spreadsheet to assist in the calculation of $\langle Eu \rangle$ for different flow and structural conditions.

Equation (17) gives the maximum non-dimensional pressure gradient for a given set of structural parameters and flow conditions. As stated previously potential flow theory does not account for the viscous effects within the boundary layer and the lee wake region; and the vertical integration does not allow for the determination of the vertical exchange in energy across the face of the structure. For this reason $\langle Eu \rangle$ by itself is not sufficient to predict the equilibrium scour depth. The remaining parameters in equation (7) are required in order to determine the influence of phenomena and processes not covered by the Euler number, as will be described later.

Database Description

A significant amount of equilibrium scour data have been published in the past. In this study published data on equilibrium scour depths around both uniform and complex cylindrical structures were selected in order to create an equilibrium scour prediction equation for clearwater scour conditions. The decision to focus on the clearwater regime was made in order to avoid data that were influenced by ripple formation upstream of the structure, which would introduce additional sediment transport scale effects. A summary of the sources and quantities of scour data is given in Table 1 and the distribution of the most important non-dimensional parameters are given in Figure 4.

The data presented include scour tests that were conducted in the clearwater regime for cohesionless sediments only. Data were included only if all relevant parameters were presented in the publication. The aforementioned parameters include the median sediment size, average flow velocity, the sediment geometric standard deviation, water depth, structural dimensions and the time to equilibrium scour. Tests were discarded if:

- they were not run for a sufficiently long period to achieve equilibrium scour. According to Melville and Chiew (1999) this is the time required to reach a scour depth in which the scour rate does not exceed 5% of the structure diameter in 24 hours; and,
- the sediment geometric standard deviation (σ_g) was greater than 1.3. This was done to avoid the effects of bed armouring.

In addition, for a limited number of structures that did not have a circular footprint the equivalent diameter was determined and used. Only one field study is included in this dataset even though there have been a large number of field studies published. The majority of field studies were excluded for three reasons:

- field measurements tend to have time-varying flows which make it difficult to determine if a given scour hole has reached the equilibrium phase;
- in most cases, naturally occurring flows in tidal or alluvial environments are high, thus forcing scour to occur in the live bed regime for at least part of the time. The extensive bed formations developed upstream of the structure and the general lowering of the bed would provide additional difficulty in generalising any information; and,

- in most cases it is not possible to monitor the scour development systematically and, therefore, it is not possible to determine if the scour hole is fully developed.

As Figure 4 shows, the majority of the data have a Froude number ranging between 0 and 0.4 which is representative of the Fr expected in most offshore locations, typically 0 to 0.2. The values of the depth-averaged Euler number are spread over the range of 0 to 1.8, showing that there is a good distribution of complex geometries, while the distribution of $\langle Eu \rangle$ is clustered around the value of 2 for the uniform cylinders which is explained by the higher pressure gradients expected for uniform cylinders extending to the water surface. In this dataset the majority of the data points have a mobility ratio (U/U_c) value close to 1 for both structure categories which yields the deepest scour for the given hydrodynamic conditions. In addition, the non-dimensional flow depth is mainly below 5 for both categories, which is typical of offshore locations where structures are constructed. Finally, the majority of the data have Reynolds numbers mainly smaller than 10^6, which is due to the lack of prototype data.

Experiment description

A series of tests were conducted to investigate the relationship between the depth-averaged Euler number of complex structure geometries and the equilibrium scour depth. These tests also gave a good opportunity to fill some gaps in the previously mentioned database. These gaps are attributed to the limited amount of published equilibrium scour depth data for non-uniform cylindrical structures which correspond to $\langle Eu \rangle \in (0.5, 1.5)$. Two sets of experiments were conducted at different structural scales. The first set were run in a reversing current flume with dimensions of 10 m x 0.3 m x 0.5 m (LxWxH). The second were conducted in a flume with dimensions of 20 m x 1.2 m x 1 m (LxWxH). The experimental apparatus in both cases consisted of a false bed that was installed around the midpoint of the flume, where the sediment was placed, and extended across the full width of the flume. A schematic of the set-up for the first set of experiments is presented in Figure 5. All tests in the present study were conducted under the forcing of a steady current. The scour depth was evaluated by the use of a scale which was marked onto the model structure (below the initial bed level) and monitored continuously by a camera taking time lapse images at an interval of 15 s.

In the first set of tests, six structural geometries were subjected to a range of different hydraulic conditions. These included three different conical base structures, one cylindrical base structure, one truncated cylinder and one uniform cylinder with the base diameter equal to that of the uniform cylinder. The second set of experiments looked at one cylinder, two conical based structures and one cylindrical based structure at scale four times larger than the first set of structures. These models were subjected to two sets of flow conditions:

- a logarithmic flow profile, in order to examine possible scale effects compared to the smaller scale experiments; and,
- a non-logarithmic flow profile with the same flow flux as in the first set, for the purpose of examining the influence non-logarithmic flow profiles have on the scour process. The flow profile was altered through a series of wire meshes in order to achieve a flow profile resembling one subject to a wind stress at the surface (profile u_2 Figure 1 a).

The smooth walled structures selected in this study are representative of geometries that have been used in the offshore wind industry details of which can be found in Figure 3.

Experiments were conducted under clearwater scour conditions in order to avoid bedform generation upstream of the structure and because clearwater scour with values of U/U_c close to 1 produces the deepest equilibrium scour (Melville and Sutherland, 1988). The structures shown in Figure 3 were subjected to a range of different flow conditions which are summarized in Figure 6. In order to avoid scaling issues due to the sediment size to pile diameter ratio (Chiew, 1984) the two sediment sizes used in the experiments were selected such that $D_{base}/d_{50} > 50$. The flow depths were also selected in order to satisfy the blockage criterion $A_{model}/A_{flow} < 1/6$ where A_{model} and A_{flow} are the cross-sectional area of the structure and the channel projected to the flow (Whitehouse, 1998).

Velocity profiles were measured at the beginning of each experiment, using a Laser Doppler Velocimeter (LDV) for the small scale experiments and an Acoustic Doppler Velocimeter (ADV) during the large scale experiments, to ensure that the same flow conditions were maintained for each experimental test. Representative profiles of the different flow conditions are shown in Figure 7 in a non-dimensional form.

Equilibrium scour depth prediction equation

On non-dimensional grounds the equilibrium scour depth for any structure and flow condition can be derived through Equation (6), assuming that the flow is incompressible and steady, that the soil consists of cohesionless particles with a low geometric standard deviation $(\sigma_g < 1.3)$ and the scour is in clearwater regime. The main goal of the proposed formula is to provide a tool that is able to predict the equilibrium scour depth around both complex and uniform structures reliably for unidirectional currents. This allows for the prediction of scour depths in alluvial environments accurately and in a conservative manner in offshore conditions as the action of waves reduces the effects of scour due to tidal action because of its ability to backfill the scour hole (Sumer et al., 2013).

In order to develop the new formula the general concept presented by Breusers et al. (1977) is adopted. This describes scour as a function of the product of the governing non-dimensional parameters (f_i) identified as influencing the process. The general form reads:

$$\frac{S}{D_{base}} = f\left(\prod_{1}^{n} f_i\right) \tag{18}$$

By performing parametric model studies, Equation (19) was selected as the most effective formula for predicting the non-dimensional scour depth.

$$\frac{S}{D_{base}} = \frac{a\,\zeta + b}{\zeta + c} \tag{19}$$

where:

$$\zeta = \left(\frac{1}{\log(Re_D)}\right)\left(\frac{h}{D_{base}}\right)(Fr)(Eu)^{0.5}\left(\frac{U}{U_c}\right)^{0.5} \tag{20}$$

a, b and c are coefficients that were determined through parameter optimisation according to McCuen and Snyder (1986). Their values for the given data-set with the corresponding 95% confidence bounds are:

$a\ =\ 2.163\ \in [2.1, 2.3]$;

$b\ =\ 0\ \in [-0.009, 0.005]$; and,

$c\ =\ 0.03\ \in [0.01, 0.05]$.

Figure 8 plots the relationship between the non-dimensional scour depth and parameter ζ. It can be observed that low values of ζ produce small equilibrium scour depths while for increasing values of ζ, S/D_{base} increases. This behaviour can be explained by the presence of D_{base} at the denominator at the right hand side of Equation (19), which implies that larger structures (in diameter) produce relatively shallower scour holes while smaller structures create deeper non-dimensional equilibrium scour depths. This is the behaviour reported by numerous authors such as Ettema et al. (2006). An example of such large experimental scour depths are the results of Chiew (1984) who measured scour depths up to S/D = 2.7. This discrepancy is attributed to the effect of the pile Reynolds number according to Ettema et al. (2006), although a number of examples have been reported in the literature (e.g. Harris and Whitehouse, 2015) where prototype scour depths were comparable to those of laboratory experiments (i.e.

S/D~1.8). In addition to the effect of the pile size several physical phenomena have also been found to contribute to the smaller scour depths in offshore locations. McGovern et al. (2014) concluded that scour in tidal flows is less than the corresponding scour induced by a unidirectional current. This conclusion was debated by Harris and Whitehouse (2015) who showed that scour depths around monopiles in offshore locations fit within the same population as scour induced around piles in unidirectional flows. This finding is also supported by Porter et al. (2015) who conducted a series of experiments and found that the scour depth between reversing and unidirectional currents does not differ. Furthermore, Sumer et al. (2012) concluded, through a series of experiments, that when the wave climate changes the equilibrium scour depth may be reduced due to a backfilling process. The previous discussion shows that there are numerous phenomena that may partially explain the observation of smaller scour depths at offshore monopoles in granular soils in some cases, but in general terms scour depths similar to those induced by unidirectional currents in rivers should be expected. It should be noted that additional research is required in order to understand the exact consequences these phenomena have on offshore scour.

During the analysis of the data the velocity profile of a number of tests from the database included in this study were not known and were assumed to be logarithmic and to follow Equation (13). This assumption, along with the fact that laboratory experiments are prone to laboratory effects such as wall friction and non-uniform flow distribution across the width of the flume, are expected to have contributed to the scatter in Figure 8.

The accuracy of the present scour prediction method is evaluated through the comparison of the predicted scour depths (using equation 19) to the corresponding measurements (Figure 9). The figure shows that a good agreement is found between the proposed method and the scour depth database compiled in this study. 55% of the predictions have an error smaller than 10% and 82% of the predictions an error smaller than 20%. The values of correlation coefficient (R^2) and RMSE (Root Mean Squared Error) were calculated to be of 0.91 and 0.16 respectively. It should be kept in mind that a factor contributing to this high accuracy is that the same database that was used to evaluate the accuracy of the model was also used to develop it. A limited number of scour predictors for complex structures are found in the literature. Most of them rely on shape factors to account for the different structure geometry (e.g. Breusers et al., 1977; Laursen and Toch, 1956). Scour prediction around GBFs can be calculated through the Khalfin (1983) method which may lead to the underestimation of the scour depth in some cases. This is because the method was derived for foundations with a limited skirt depth. Others provide a conservative method of estimating the equilibrium scour depth through envelope curves (i.e. FDOT, 2005) which leads to the overestimation of the scour depths in some cases. Thus the present equation may be a good solution for providing a basis for the deterministic and probabilistic assessment of scour, which cannot be done with the other prediction methods.

Behaviour of scour prediction equation

Having derived the scour prediction formula, the contribution of different physical factors to its behaviour are assessed.

Influence of depth averaged Euler number

Given that the viscous forces in the flow-structure interaction around piers are negligible, one needs to find a non-dimensional quantity to describe the flow alteration upstream of the structure. This implies that a variable that includes the structure length scale and some form of the kinetic energy is required. The depth-averaged pressure gradient in the form of the Euler number, described earlier in this paper, includes both of these physical quantities, and hence it should be possible to describe the two main mechanisms driving the scour process, which are present upstream of the structure. The first of these is the horseshoe vortex and the second is the flow acceleration. Potential flow theory suggests that, given the flow conditions remain constant, an increasing blockage induced by a structure would result in a larger amplification of the adverse pressure gradient and thus an increase in the local scour potential. The experiments conducted in the current study were designed to test this hypothesis and yield results which relate the depth-averaged Euler number to the equilibrium scour depth for different structures. Figures 10 through 12 show the influence that the pressure gradient has on the equilibrium scour depth for different ranges of sediment mobility parameter, flow depth and velocity profiles. In these figures the different colours denote a different type of structure while the different symbols correspond to the different flow conditions. Figure 10 shows the influence of $\langle Eu \rangle$ on the equilibrium scour depth for test series 1.1 through 1.29 and the lines correspond to the prediction given by Equation (19) for the corresponding flow conditions. It shows that an increasing Euler number yields an increase in the equilibrium scour depth given that the remaining flow conditions are the same and it reaches an asymptotic value of S/D as $\langle Eu \rangle$ approaches 2.

Further observation of Figures 10 and 11 shows that tests conducted with different sediment sizes but having the same sediment mobility number do not differ significantly with regards to the equilibrium scour depth. In addition, a decrease in the mobility parameter (U/U_c) or (h/D_{base}) results in the same trend described above with respect to $\langle Eu \rangle$, but with the horizontal asymptote shifting to a lower value of S/D_{base} .

Figure 12 shows the results from the larger scale scour tests. It can be observed that the equilibrium scour depth increases as $\langle Eu \rangle$ increases in the same manner as for the smaller scale tests. Furthermore, the data for complex foundation shapes corresponding to the non-logarithmic flow profile are shifted further to the left compared to the tests that were subjected to the logarithmic flow profile, while both test results fall onto the same trend line. The effect of the non-logarithmic profile on scour for the monopile is less than for the complex foundation shapes. Given that the depth-averaged flow velocity in both cases is the same, lower flow velocities are observed near the bed in the case of the non-logarithmic profile case. This translates to less kinetic energy interacting with the larger base which yields smaller $\langle Eu \rangle$ and thus smaller scour depths. In addition, given that all of the remaining non-dimensional flow parameters listed in equation (7) are kept constant during the two tests, it is also expected that both results fall on to the same curve defined by equation (19). Finally, even though the larger scale data plotted in Figure 12 were derived from experiments with slightly different values of the non-dimensional water depth, mobility ratio and Fr, it can be observed that an increase in the structural scale of each of the foundation models results in a significant decrease in the non-dimensional equilibrium scour depth. This effect is linked to the different pile Reynolds number this set of tests has, and will be elaborated on further in the following section.

Influence of pile Reynolds number

During the large scale experiment two main sediment transport systems were identified:

- the sediment from the upstream region of the structure was transported and deposited at the lee of the structure at an angle 160°-200° relative to the flow direction. This process is primarily induced by the local increase in the horseshoe vortex in front of the structure and thus described by the change in Eu, h/D and Fr; and,
- a secondary process that suspends the previously deposited sediment at the lee of the structure into the water column, which is then carried away from the scour hole and deposited further downstream from the structure. This process is mainly driven by the longitudinal counter-rotating vortices which are created partly by the horseshoe vortex and the variation of the shedding frequency over the height of the structure (Baykal et al., 2015; Petersen et al., 2015; Kirkil and Constantinescu, 2010). Thus this process should be characterised by the pile Reynolds number.

This finding is presented in Figure 13, and shows that the pile Reynolds number is an important factor controlling the scour process. According to Schlichting (1979) the size of the pile wall boundary layer is proportional to $1/ln(Re_D)$ which means that the overall turbulence induced by the flow-structure interaction would decrease as the Reynolds number increases. In addition Achenbach (1968) showed that an increasing Re_D forces the separation point to shift further downstream of the pile, which also would result in a decrease in the sediment transport capacity of the lee wake vortices and thus decrease the overall scour potential. This shows that Re_D could account for some scale effects that result in smaller non-dimensional scour depths for larger scale structures.

To demonstrate this effect Figure 13 shows the influence of Re_D ($10^3 \le Re_D \le 4\ 10^6$) on the equilibrium scour depth for varying Re_D. The data points in this figure correspond to scour tests (from the dataset presented in this study) in which the remaining flow parameters did not vary significantly $Fr = \{0.15 - 0.20\}$, $U/U_c = \{0.7 - 0.85\}$, $h/D = \{2 - 3\}$ and $\langle Eu \rangle = \{1.7 - 2\}$. As can be observed in the figure an increasing pile Reynolds number does indeed have the effect of decreasing the non-dimensional equilibrium scour depth. This trend is captured relatively well by the scour prediction equation given in (19) over a wide range of Re_D.

An increase in the flow velocity or the diameter of the structure would also change the other non-dimensional parameters found in equation (19) in addition to the pile Reynolds number. For instance, an increase in the mean flow velocity would also increase the sediment mobility number and the Froude number. The combined effect of an increase in the mean flow velocity and the pile diameter was investigated by Shen et al. (1969). In the study the influence of the pile Reynolds number was explored. The experiments were conducted for a circular pier with diameters ranging from 0.15m to 0.9m and a median sand diameter of 0.24mm under the forcing of a unidirectional current with different flow velocities $0.3 < U/U_c < 3$. A best fit equation was then obtained by combining the test results with other published data with similar non-dimensional flow depths and pile diameters, which resulted in the following equilibrium scour depth prediction equation:

$$S = 0.00022 {Re_D}^{0.619}\ (S.I.units) \qquad (21)$$

In Figure 14 a comparison of the present equation (equation 19) and equation (21) is shown for data compiled over a more limited range of Re_D in the centre of the Figure 13 range The prediction equations are plotted against the equilibrium scour depth data compiled by Breusers et al. (1977) which were obtained from Sheppard et al. (2011). In this figure only the clearwater scour data are plotted, as live bed scour is outside the scope of this study. As can be seen the two equations show a similar agreement with the clearwater scour data for $Re_D < 4 * 10^4$. In the same figure it can be observed that the equation in Shen et al. (1969) equation shows a tendency to give a better prediction of the Chabert and Engeldinger (1956) data, while equation (19) shows a better agreement with the data of Shen et al., 1969 for larger Re_D. At the lower Reynolds number range the methods tend to underpredict, and this may be related to the comment by Sheppard et al. (2011), that the Chabert and Engeldinger data in the range $U/U_c < 0.7$ tend to feature much deeper scour than other datasets.

Influence of Froude number

According to numerous authors (e.g. Baker, 1986; Graf and Yulistiyanto, 1998) a significant process that controls the scour process is the strength of the horseshoe vortex. On physical grounds it can be understood that the intensity of the horseshoe vortex should be strongly influenced by the downflow at the face of the structure. Based on the Bernoulli equation and the conservation of energy it can be concluded that the downflow is dependent on both the hydrostatic component and the kinetic component of the energy. Therefore, by applying the Bernoulli equation from a location far away from the structure (where the flow field is undisturbed) to its leading face, we can obtain:

$$\frac{y}{h} \propto Fr^{e} \tag{22}$$

where y is the vertical location of the stagnation point (see Figure 15) along the face of the structure and e is a constant.

Figure 16 shows the influence of the Froude number on the equilibrium scour depth for a subset of the data presented in Table 1. In this figure the depicted data points have values of the Froude number ranging from 0.11 to 0.97 while $Re_D = \{75000 - 150000\}, U/U_c = \{0.8 - 1\}, h/D = \{2 - 3\}$ and $\langle Eu \rangle = \{1.7 - 2\}$. It can be observed that the scour depth increases following a logarithmic trend and reaches a horizontal asymptote as $Fr \rightarrow \infty$. This means that for shallow water depths the high Froude number results in a stronger kinetic component of the pressure field and, therefore, in a stagnation point which is closer to the water surface. Thus a larger portion of the flow is “captured” by the downflow which results in deeper scour depths. On the other hand greater flow depths result in smaller Froude numbers which means that the hydrodynamic component of the pressure force is larger, effectively creating a more evenly distributed pressure field along the face of the structure and thus leading to a vertical stagnation point closer to the bed and, therefore, smaller scour depths (Harris and Whitehouse, 2015).

Influence of non-dimensional flow depth

The flow depth also influences the scour depth in a way that cannot be captured by the Froude number. According to Sumer and Fredsøe (2002) the boundary layer separation at the bed will be delayed if the non-dimensional water depth is small, as a smaller h/D would result in a more uniform flow distribution. This in turn will result in a smaller horseshoe vortex and, therefore, in a smaller scour potential. Figure 17 shows the influence of the water depth on the non-dimensional scour depth for data where the rest of the flow conditions do not vary significantly; $Re_D = \{100000 - 300000\}, U/U_c = \{0.8 - 1\}, Fr = \{0.1 - 0.25\}$ and $\langle Eu \rangle = \{1.7 - 2\}$.

In reality a change in the water depth (h) would affect both the Froude number and the non-dimensional flow depth (h/D). According to the discussion presented in the previous sections, an increase in the flow depth would decrease the Froude number and increase h/D. The combined effect of a change in the water depth while maintaining the values of the remaining parameters constant is demonstrated in Figure 18, where the clearwater equilibrium scour depth data compiled by Melville and Sutherland (1988) is also plotted. It can be observed that Equation (19) captures the trend of their data well, albeit with a tendency to over-predict the scour depths for $0.5 < h/D < 1.5$.

Influence of the sediment mobility ratio

As mentioned earlier the sediment mobility ratio significantly effects the equilibrium scour depth potential for a given structure and flow conditions. In the context of the equilibrium scour Equation (19), U/U_c is a factor that describes the resistance of the local bed to the hydrodynamic forces that are amplified due to the presence of the structure. The importance of the sediment mobility ratio on physical grounds can be obtained by applying the 2D-Vertical continuity equation at a control volume extending from a location upstream of the scour hole to the deepest point of the scour hole and assuming that at the equilibrium phase of scour the incoming flow into the scour hole is U and the mean flow velocity at the deepest point of the scour hole is U_c, leading to Equation (23):

$$\frac{S}{D} = d\left(\frac{U}{U_c}\right) \; for \; U \leq U_c \tag{23}$$

in which variable d is a function of the length of the scour hole in the streamwise direction at equilibrium and the structure's diameter.

Figure 19 demonstrates the effect of the mobility parameter on the equilibrium scour for a set of data where U/U_c varies between 0.35 and 0.99 and $Re_D = \{50000 - 200000\}, h/D = \{3 - 6\}, Fr = \{0.1 - 0.15\}$ and $\langle Eu \rangle = \{1.7 - 2\}$. The data show reasonably good agreement with Equation (19) and with the observations reported by Melville and Sutherland (1988) who analysed the data of Baker (1986).

Conclusions

In this research a design method for the prediction of the equilibrium scour depth around uniform and non-uniform cylindrical structure geometries under clearwater scour conditions is presented. The equation is derived based on experimental and field data obtained by experiments in this study and other published work. This method is based on a new physical quantity, the depth-averaged Euler number, the influence of which is verified through experimental data collected during this research. Other influencing physical quantities that have been identified in this study are Re_D, Fr, U/U_c and h/D. The importance and influence has been explained through experimental data and on physical grounds.

Acknowledgements

Appreciation is recorded for the financial support and expertise provided by HR Wallingford and the Engineering & Physical Sciences Research Council for the grant funding this research. JMH and RJSW acknowledge funding from HR Wallingford's strategic research programme.

Notation

A = constant;

A_{model} = cross-sectional area of model projected to the flow;

A_{flow} = cross-sectional area of channel projected to the flow;

a = constant;

b = constant;

c = constant;

D = diameter of pile;

D_{base} = diameter of base in a structure;

d_{50} = median grain diameter;

D_* = dimensionless grain size;

d = constant;

$dp/d\varphi$ = pressure gradient at any given location around the structure;

$\langle dp/d\varphi \rangle$ = depth averaged pressure gradient at any given location around the structure;

Eu = Euler number;

$\langle Eu \rangle$ = depth averaged Euler number;

e = constant;

Fr = Froude number;

f_i = non dimensional quantity influencing scour;

g = gravitational acceleration;

h = flow depth;

K_i = product of all correction factors;

k_s = Nikuradse roughness length scale;

p = pressure;

R = the radius of the structure;

R^2 = Squared multiple correlation coefficient;

Re = Reynolds Number;

Re_D = pile Reynolds Number;

Re_* = grain Reynolds Number;

r = radial distance from the pier centre where the pressure gradient is evaluated;

S = equilibrium scour depth;s = ratio of densities of grains and water;

U = depth averaged flow velocity;

U_c = critical velocity for bed sediment movement;

U_f = friction velocity based on the average velocity and sediment size;

u_φ = tangential component of the velocity in polar coordinates with origin the centre of the structure;

u_r = radial component of the velocity in polar coordinates with origin the centre of the structure;

y = vertical distance of the stagnation point from the bed

Y = vertical distance of the top of the pile cap from the bed

z = vertical distance from bed;γ = specific gravity of water;

$\zeta = \left(\frac{1}{\log(Re_D)}\right)\left(\frac{h}{D_{base}}\right)(Fr)(Eu)^{0.5}\left(\frac{U}{U_c}\right)^{0.5}$;

θ_c = critical shields number

μ = dynamic viscosity of water;

ν = kinematic viscosity of water;

ρ = density of water;

σ_g = geometric standard deviation of sediment (d84/d16; ratio of 84th and 16th percentile in size grading); and,

φ = angle relative to the flow direction.

References

Achenbach, E. (1968). Distribution of local pressure and skin friction around a circular cylinder in cross-flow up to Re= 5× 10 6. *Journal of Fluid Mechanics*, 34(04), 625-639.

Amini, A., Melville, B. W., and Ali, T. M. (2014). Local scour at piled bridge piers including an examination of the superposition method. *Canadian Journal of Civil Engineering*, *41*(5), 461-471.

Ataie-Ashtiani, B., Z. Baratian-Ghorghi, and A. A. Beheshti. (2010). Experimental investigation of clear-water local scour of compound piers. *Journal of Hydraulic Engineering* 136.6 : 343-351.

Baker, R. E. (1986). *Local scour at bridge piers in non-uniform sediment*. Univ. of Auckland, Auckland, New Zealand.

Baykal, C., Sumer, B. M., Fuhrman, D. R., Jacobsen, N. G., and Fredsøe, J. (2015). Numerical investigation of flow and scour around a vertical circular cylinder. *Philosophical Transactions of the Royal Society of London A: Mathematical, Physical and Engineering Sciences, 373(2033)*, 20140104.

Bos, K.J., Chen, Z., Verheij, H.J., Onderwater, M. and Visser, M. (2002). Local scour and scour protection of F3 offshore GBS platform. *Proceedings OMAE'02 21st International Conference on Ocean, Offshore and Arctic Engineering*, Paper 28127, June 23-28, 2002, Oslo, Norway.

Breusers, H. N. C., Nicollet, G., and Shen, H. W. (1977). Local scour around cylindrical piers. *Journal of Hydraulic Research*, 15(3), 211-252.

Chabert, J., and Engeldinger, P. (1956). *Study of scour around bridge piers*. Rep. Prepared for the Laboratoire National d'Hydraulique.

Chiew, Y. M. (1984). *Local scour at bridge piers*. Univ. of Auckland, Auckland, New Zealand.

Davies, A. M. and Lawrence, J. (1994). Examining the Influence of Wind and Wind Wave Turbulence on Tidal Currents, Using a Three-Dimensional Hydrodynamic Model Including Wave–Current Interaction. *Journal of Physical Oceanography*, 24:12, 2441-2460

Dey, S., Bose, S. K., and Sastry, G. L. (1995). Clear water scour at circular piers: a model. *Journal of Hydraulic Engineering*, 121(12), 869-876.

Einstein, H. A. (1950). The Bed-Load Function for Sediment Transportation. *Open Channel Flow Technical Bulletin No*, 1026.

Ettema, R. (1980). *Scour at bridge piers*. Rep. No. 216, Univ. of Auckland, Auckland, New Zealand.

Ettema, R., Kirkil, G., and Muste, M. (2006). Similitude of large-scale turbulence in experiments on local scour at cylinders. *Journal of Hydraulic Engineering*, 132(1), 33-40.

Ferraro, D., Tafarojnoruz, A., Gaudio, R., and Cardoso, A. H. (2013). Effects of pile cap thickness on the maximum scour depth at a complex pier. *Journal of Hydraulic Engineering*, *139*(5), 482-491.

Florida department of transportation. (2005). *Bridge scour manual.* Tallahassee, Florida, United States.

Graf, W. H., and Yulistiyanto, B. (1998). Experiments on flow around a cylinder; the velocity and vorticity fields. *Journal of Hydraulic Research*, 36(4), 637-654.

Harris, J.M. and Whitehouse, R.J.S. (2015). Marine scour: Lessons from Nature's laboratory. *In: Scour and Erosion, Proc. 7th Int. Conf. on Scour and Erosion*, The University of Western Australia, 2 - 4 December, 2014, (eds.) Cheng. L., Draper, S. and An, H., CRC Press, p. 19 - 31(Keynote).

Hoffmans, G. J.C.M., and Verheij, H. J. (1997). *Scour manual*. (Vol. 96). CRC Press.

Hughes, S. A. (1993). *Physical models and laboratory techniques in coastal engineering* (Vol. 7). World Scientific.

Jannaty, M. H., Eghbalzadeh, A., & Hosseini, S. A. (2015). Using field data to evaluate the complex bridge piers scour methods. *Canadian Journal of Civil Engineering*, 43(3), 218-225.

Jain, S. C., and Fischer, E. E. (1979). *Scour around circular bridge piers at high Froude numbers*. (No. FHWA-RD-79-104 Final Rpt.).

Johnson, P. A. (1992). Reliability-based pier scour engineering. *Journal of Hydraulic Engineering, 118(10)*, 1344-1358.

Jones, J. S., Kilgore, R. T., and Mistichelli, M. P. (1992). Effects of footing location on bridge pier scour. *Journal of Hydraulic Engineering*, 118(2), 280-290.

Khalfin, I. S. (1983). Local scour around ice-resistant structures caused by wave and current effect. In: *Proc. The Seventh International Conference on Port and Ocean Engineering under Arctic Conditions*, Helsinki, Finland (Vol. 2, pp. 992-1002).

Kirkil, G. and Constantinescu, G. (2010) “Flow and Turbulence Structure around an In-stream Rectangular Cylinder with Scour Hole.” *Water Resources Research*, 46, W11549.

Laursen, E. M., and Toch, A. (1956). *Scour around bridge piers and abutments* (Vol. 4). Ames, IA, USA: Iowa Highway Research Board.

McGovern, D. J., Ilic, S., Folkard, A. M., McLelland, S. J., and Murphy, B. J. (2014). Time development of scour around a cylinder in simulated tidal currents. *Journal of Hydraulic Engineering*, 140(6), 04014014.

Melville, B. W., and Sutherland, A. J. (1988). Design method for local scour at bridge piers. *Journal of Hydraulic Engineering*, 114(10), 1210-1226.

Melville, B. W., and Raudkivi, A. J. (1996). Effects of foundation geometry on bridge pier scour. *Journal of Hydraulic Engineering*, 122(4), 203-209.

Melville, B. W. (1997). Pier and abutment scour: integrated approach. *Journal of Hydraulic Engineering*, 123(2), 125-136.

Melville, B. W., and Chiew, Y. M. (1999). Time scale for local scour at bridge piers. *Journal of Hydraulic Engineering*, 125(1), 59-65.

Melville, B. (2008). The physics of local scour at bridge piers. *Proceedings of Fourth International Conference on Scour and Erosion, Tokyo* (pp. 28-38).

Moreno, M., Maia, R., and Couto, L. (2015). Effects of Relative Column Width and Pile-Cap Elevation on Local Scour Depth around Complex Piers. *Journal of Hydraulic Engineering*, 04015051.

Matutano, C., Negro, V., López-Gutiérrez, J. S., and Esteban, M. D. (2013). Scour prediction and scour protections in offshore wind farms. *Renewable Energy*, *57*, 358-365.

Parola, A. C., Mahavadi, S. K., Brown, B. M., and El Khoury, A. (1996). Effects of rectangular foundation geometry on local pier scour. *Journal of Hydraulic Engineering*, *122*(1), 35-40.

Petersen, T.U., Sumer, B.M., Fredsøe, J., Raaijmakers, T. and Schouten, J. (2015): "Edge scour at scour protection around piles in the marine environment - Laboratory and field Investigation". *Coastal Engineering*, 106 (2015) 42-72.

Porter, K., Harris, J., and Simons, R. (2015). Discussion of "Time Development of Scour around a Cylinder in Simulated Tidal Currents" by David J. McGovern, Suzana Ilic, Andrew M. Folkard, Stuart J. McLelland, and Brendan J. Murphy. *Journal of Hydraulic Engineering*, 141(7).

Roulund, A., Sumer, B. M., Fredsøe, J., and Michelsen, J. (2005). Numerical and experimental investigation of flow and scour around a circular pile. *Journal of Fluid Mechanics, 534*, 351-401.

Schlichting, H. T., and Truckenbrodt, E. A. (1979). *Aerodynamics of the Airplane*. McGraw-Hill Companies.

Sarpkaya, T. (2010). *Wave forces on offshore structures*. Cambridge University Press.

Shen, H. W., Schneider, V. R., and Karaki, S. (1969). Local scour around bridge piers. *Journal of the Hydraulics Division*, 95(6), 1919-1940.

Sheppard, D. M., Odeh, M., and Glasser, T. (2004). Large scale clear-water local pier scour experiments. *Journal of Hydraulic Engineering*, 130(10), 957-963.

Sheppard, D. M., and Miller Jr, W. (2006). Live-bed local pier scour experiments. *Journal of Hydraulic Engineering*, 132(7), 635-642.

Sheppard, D. M., Demir, H., and Melville, B. W. (2011). *Scour at wide piers and long skewed piers (Vol. 682)*. Transportation Research Board.

Simons, R.R., Weller, J. and Whitehouse, R.J.S. (2009). Scour development around truncated cylindrical structures. *Coastal Structures 2007, Proceedings of the 5th Coastal Structures International Conference*, CSt07, Venice, Italy.

Soulsby, R. (1997). *Dynamics of marine sands: a manual for practical applications*. Thomas Telford.

Sumer, B. M., and Fredsøe, J. (2002). *The mechanics of scour in the marine environment*. World Scientific.

Sumer, B. M., Petersen, T. U., Locatelli, L., Fredsøe, J., Musumeci, R. E., and Foti, E. (2013). Backfilling of a scour hole around a pile in waves and current. *Journal of Waterway, Port, Coastal, and Ocean Engineering*, 139(1), 9-23.

Tavouktsoglou, N.S., Harris, J.M., Simons, R.R. and Whitehouse, R.J. (2015). Bed shear stress distribution around offshore gravity foundations. *Proceedings of the ASME 2015 34th International Conference on Ocean, Offshore and Arctic Engineering*, OMAE2015, St. John's Newfoundland, Canada, May 31 – June 5, Paper No. OMAE2015-41966, American Society of Mechanical Engineers, pp. V007T06A051-V007T06A051.

Tavouktsoglou, N. S., Harris, J. M., Simons, R. R., and Whitehouse, R. J. (2016). Equilibrium scour prediction for uniform and non-uniform cylindrical structures under clear water conditions. *Proceedings of the ASME 2016 35th International Conference on Ocean, Offshore and Arctic Engineering*, OMAE2016, Busan, South Korea, June 19-24, Paper No. OMAE2016-54377, American Society of Mechanical Engineers, pp. V001T10A007-V001T10A007.

Teramoto, S., Yatagai, K., Murase, Y., Ninomiya, K., and Tagya, K. (1973). *Study on scouring of sit-on-bottom type offshore structure*. Mitsubishi Heavy Industries Technical Review, 10(1).

Whitehouse, R. (1998). *Scour at marine structures: A manual for practical applications*. Thomas Telford.

Whitehouse, R. J., Sutherland, J., and Harris, J. (2011). Evaluating scour at marine gravity foundations. *Proceedings of the ICE-Maritime Engineering*,*164*(4), 143-157.

Yanmaz, A. M., and Altinbilek, H. D. (1991). Study of time-dependent local scour around bridge piers. *Journal of Hydraulic Engineering*, 117(10), 1247-1268.

Yeow, K., and Cheng, L. (2003). Local scour around a vertical pile with a caisson foundation. In: *Proceedings of the 2nd International Conference of Asian and Pacific Coasts*.

Tables

Table 1: Summary of sources populating the scour database.

Data Source	Number of data points
Complex geometries	
Amini et al. (2014)	6
Ataie-Ashtiani et al (2010)	8
Ferraro et al (2013)	10
Hoffmans and Verheij (1997)	1
Jannaty et al (2015)	2
Melville and Raudkivi (1996)	7
Moreno et al (2015)	8
Parola et al (1996)	13
Present study	40
Simons et al (2009)	4
Whitehouse et al. (2011)	2
Total complex geometries	101
Uniform Cylinders	
Chabert and Engeldinger (1956)	85
Dey et al (1995)	18
Ettema (1980)	70
Ettema et al (2006)	5
Jain and Fischer (1979)	26
Melville (1997)	5
Melville and Chiew (1999)	12
Mututano et al (2013)	10
Shen et al (1969)	16
Sheppard and Miller (2006)	4
Sheppard et al (2004)	4
Yanmaz and Altinbilek (1991)	14
Total uniform cylinders	269

Fig. 1. Definition sketch of main parameters: (a) side view; (b) top view.

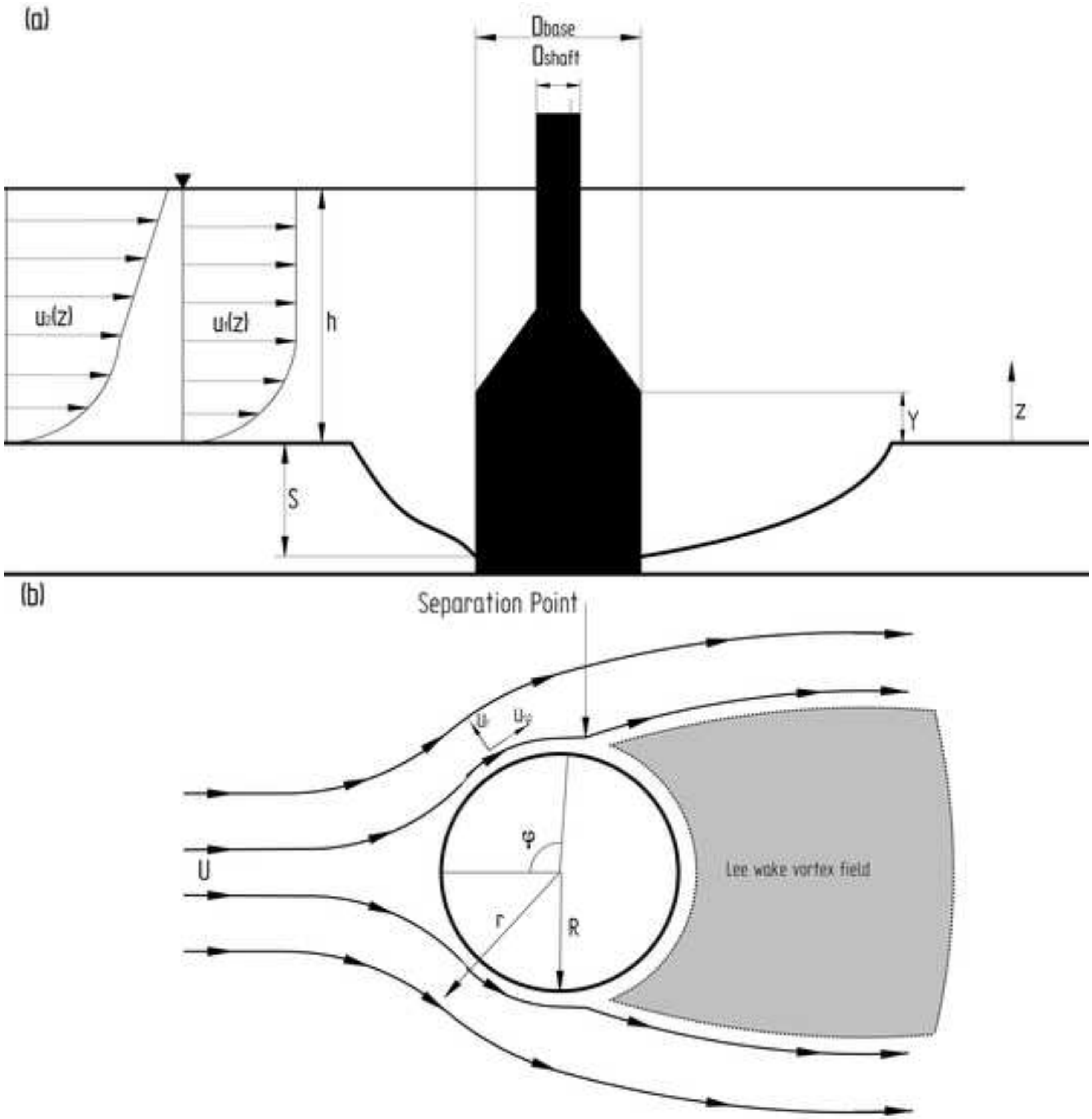

Fig. 2. Pressure gradient distribution through the water column (calculated using Equation 11) for two different structures under the same flow conditions.

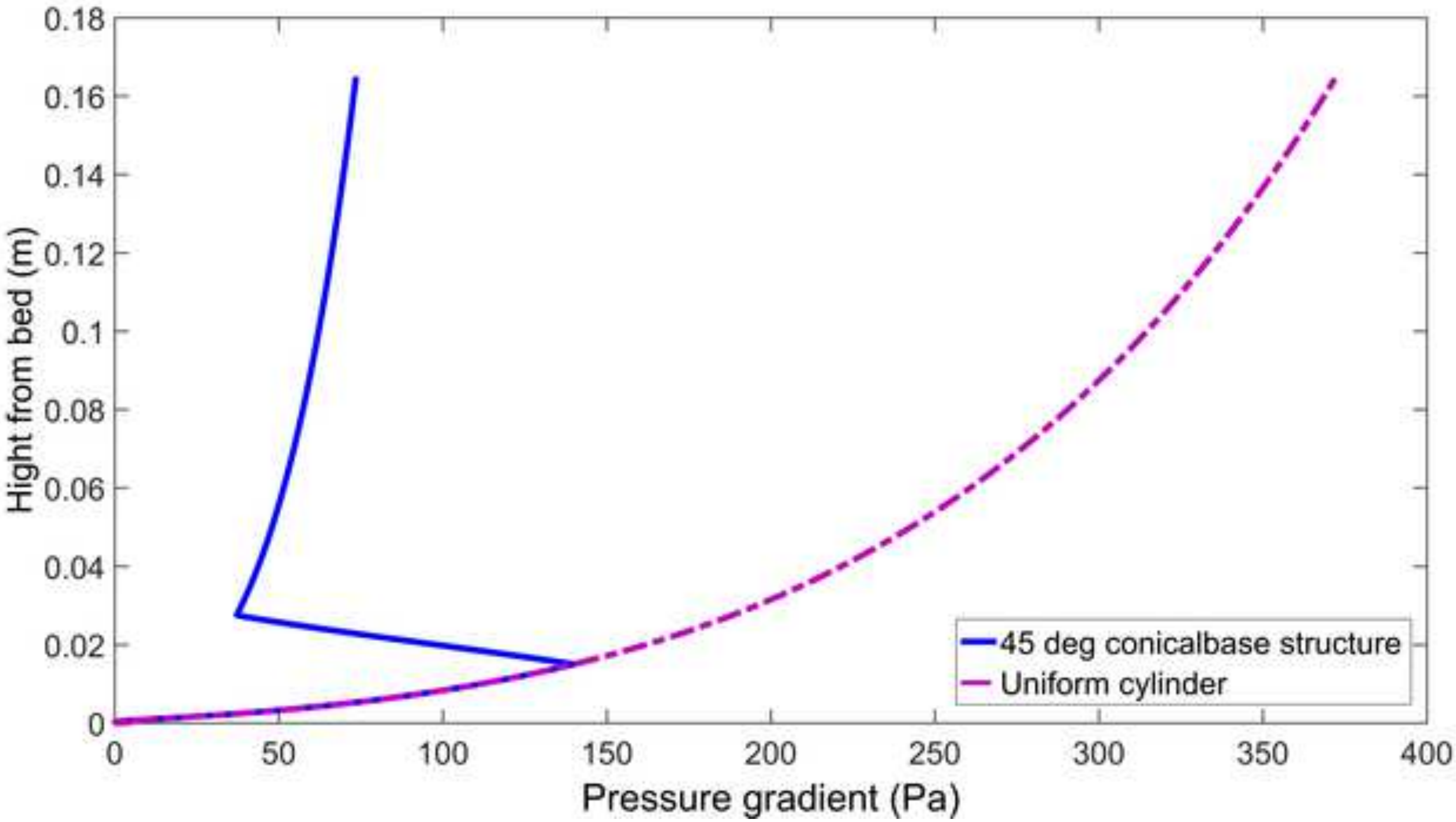

Fig. 3. Structure geometries used in this study (geometries shown in this figure include the part of the structure protruding from the original bed level).

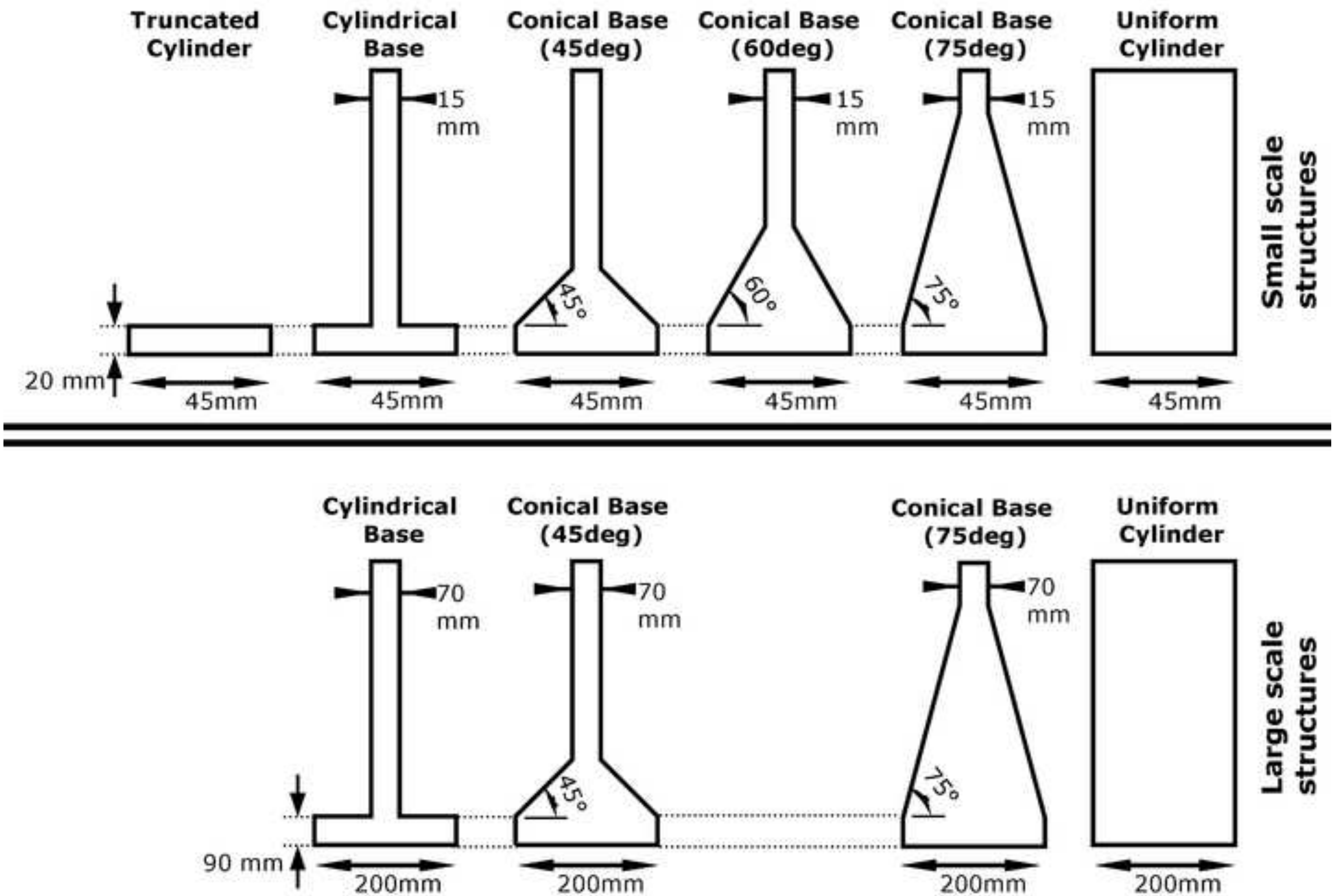

Fig. 4. Percent distribution of non-dimensional quantities in database.

Click here to download Figure Fig. 4.tif

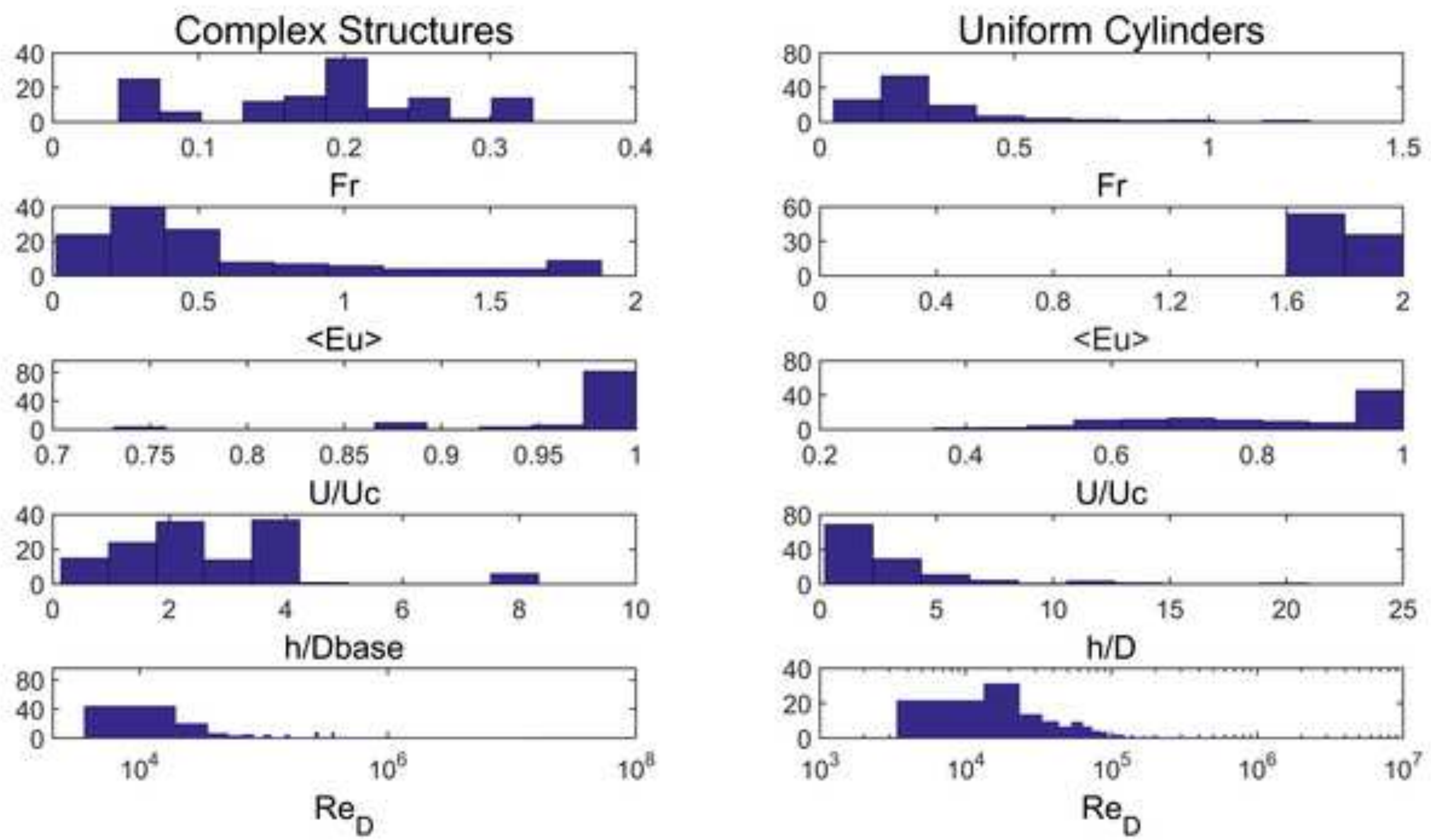

Fig. 5. Layout of flume (top: top view; bottom side view).

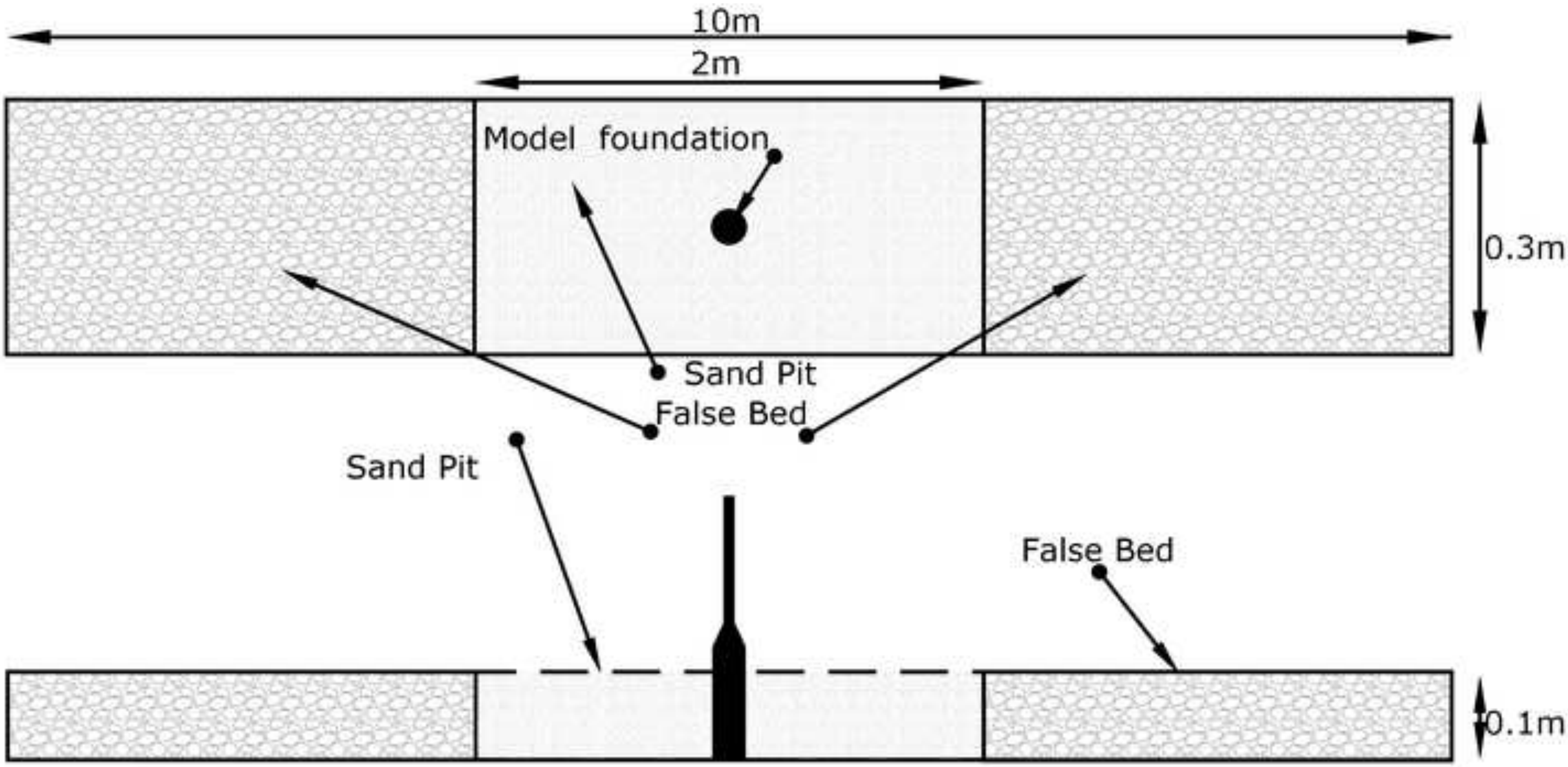

Fig. 6. Summary of flow conditions used in the test series.

Click here to download Figure Fig. 6.tif

No. (-)	Symbol	Structure Type (-)	U (m/s)	Flow Profile (-)	h (m)	D50 (mm)	h/D_{base} (-)	Re_D (-)	Eu (-)	Fr (-)
1.1	✶	Cylindrical base	0.195	logarithmic	0.165	0.6	3.67	8775	0.24	0.15
1.2	✶	45 deg conical base	0.195	logarithmic	0.165	0.6	3.67	8775	0.27	0.15
1.3	✶	60 deg conical base	0.195	logarithmic	0.165	0.6	3.67	8775	0.30	0.15
1.4	✶	75 deg conical base	0.195	logarithmic	0.165	0.6	3.67	8775	0.39	0.15
1.5	✶	Uniform cylinder	0.195	logarithmic	0.165	0.6	3.67	8775	1.70	0.15
1.6	▲	Truncated	0.2	logarithmic	0.165	0.2	3.67	9000	0.12	0.16
1.7	▲	Cylindrical base	0.2	logarithmic	0.165	0.2	3.67	9000	0.25	0.16
1.8	▲	45 deg conical base	0.2	logarithmic	0.165	0.2	3.67	9000	0.29	0.16
1.9	▲	60 deg conical base	0.2	logarithmic	0.165	0.2	3.67	9000	0.32	0.16
1.10	▲	75 deg conical base	0.2	logarithmic	0.165	0.2	3.67	9000	0.42	0.16
1.11	▲	Uniform cylinder	0.2	logarithmic	0.165	0.2	3.67	9000	1.74	0.16
1.12	●	Truncated	0.237	logarithmic	0.165	0.2	3.67	10665	0.12	0.19
1.13	●	Cylindrical base	0.237	logarithmic	0.165	0.2	3.67	10665	0.25	0.19
1.14	●	45 deg conical base	0.237	logarithmic	0.165	0.2	3.67	10665	0.29	0.19
1.15	●	60 deg conical base	0.237	logarithmic	0.165	0.2	3.67	10665	0.32	0.19
1.16	●	75 deg conical base	0.237	logarithmic	0.165	0.2	3.67	10665	0.42	0.19
1.17	●	Uniform cylinder	0.237	logarithmic	0.165	0.2	3.67	10665	1.74	0.19
1.18	★	Truncated	0.235	logarithmic	0.165	0.6	3.67	10575	0.12	0.18
1.19	★	Cylindrical base	0.235	logarithmic	0.165	0.6	3.67	10575	0.24	0.18
1.20	★	45 deg conical base	0.235	logarithmic	0.165	0.6	3.67	10575	0.27	0.18
1.21	★	60 deg conical base	0.235	logarithmic	0.165	0.6	3.67	10575	0.30	0.18
1.22	★	75 deg conical base	0.235	logarithmic	0.165	0.6	3.67	10575	0.39	0.18
1.23	★	Uniform cylinder	0.235	logarithmic	0.165	0.6	3.67	10575	1.70	0.18
1.24	■	Truncated	0.264	logarithmic	0.165	0.6	3.67	11880	0.12	0.21
1.25	■	Cylindrical base	0.264	logarithmic	0.165	0.6	3.67	11880	0.24	0.21
1.26	■	45 deg conical base	0.264	logarithmic	0.165	0.6	3.67	11880	0.27	0.21
1.27	■	60 deg conical base	0.264	logarithmic	0.165	0.6	3.67	11880	0.30	0.21
1.28	■	75 deg conical base	0.264	logarithmic	0.165	0.6	3.67	11880	0.39	0.21
1.29	■	Uniform cylinder	0.264	logarithmic	0.165	0.6	3.67	11880	1.70	0.21
2.1	◀	Truncated	0.196	logarithmic	0.1	0.2	2.22	8820	0.30	0.20
2.2	◀	Cylindrical base	0.196	logarithmic	0.1	0.2	2.22	8820	0.33	0.20
2.3	◀	45 deg conical base	0.196	logarithmic	0.1	0.2	2.22	8820	0.40	0.20
2.4	◀	60 deg conical base	0.196	logarithmic	0.1	0.2	2.22	8820	0.46	0.20
2.5	◀	75 deg conical base	0.196	logarithmic	0.1	0.2	2.22	8820	0.64	0.20
2.6	◀	Uniform cylinder	0.196	logarithmic	0.1	0.2	2.22	8820	1.72	0.20
2.7	◆	Truncated	0.193	logarithmic	0.1	0.6	2.22	8685	0.27	0.19
2.8	◆	Cylindrical base	0.193	logarithmic	0.1	0.6	2.22	8685	0.30	0.19
2.9	◆	45 deg conical base	0.193	logarithmic	0.1	0.6	2.22	8685	0.36	0.19
2.10	◆	60 deg conical base	0.193	logarithmic	0.1	0.6	2.22	8685	0.42	0.19
2.11	◆	75 deg conical base	0.193	logarithmic	0.1	0.6	2.22	8685	0.59	0.19
2.12	◆	Uniform cylinder	0.193	logarithmic	0.1	0.6	2.22	8685	1.68	0.19
3.1	▼	Cylindrical base	0.25	logarithmic	0.35	0.2	1.75	50000	0.64	0.13
3.2	▼	45 deg conical base	0.25	logarithmic	0.35	0.2	1.75	50000	0.78	0.13
3.3	▼	75 deg conical base	0.25	logarithmic	0.35	0.2	1.75	50000	1.26	0.13
3.4	▼	Uniform cylinder	0.25	logarithmic	0.35	0.2	1.75	50000	1.97	0.13
3.5	▶	Cylindrical base	0.25*	non-logarithmic	0.35	0.2	1.75	50000	0.55	0.13
3.6	▶	45 deg conical base	0.25*	non-logarithmic	0.35	0.2	1.75	50000	0.68	0.13
3.7	▶	75 deg conical base	0.25*	non-logarithmic	0.35	0.2	1.75	50000	1.15	0.13
3.8	▶	Uniform cylinder	0.25*	non-logarithmic	0.35	0.2	1.75	50000	1.84	0.13

Fig. 7. Representative non-dimensional flow profiles for the seven different flow conditions used in these experiments. (see Figure 6 for symbols).

Click here to download Figure Fig. 7.tif

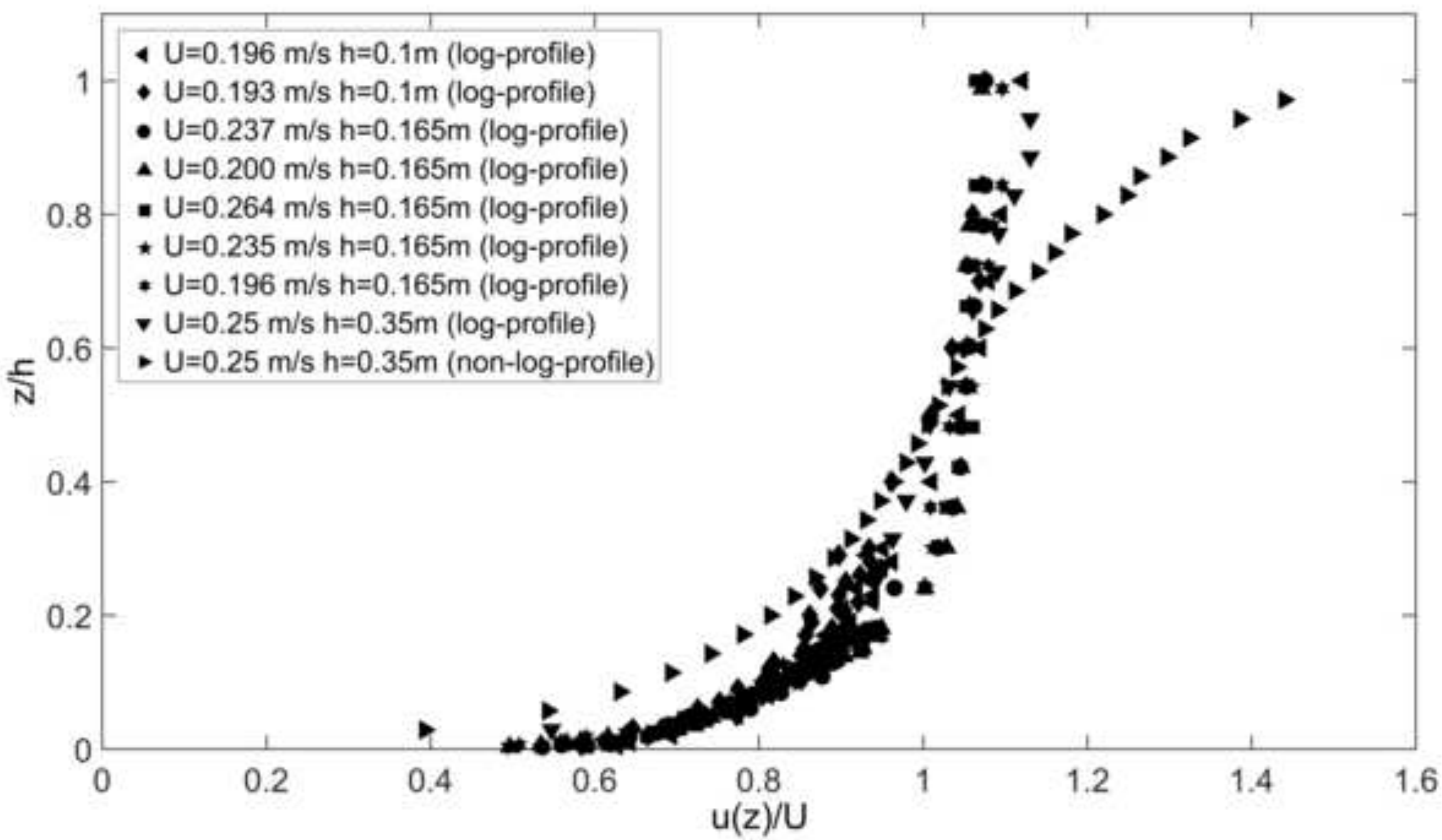

Fig. 8. Agreement between non-dimensional scour depth and ζ. Click here to download Figure Fig. 8.tif

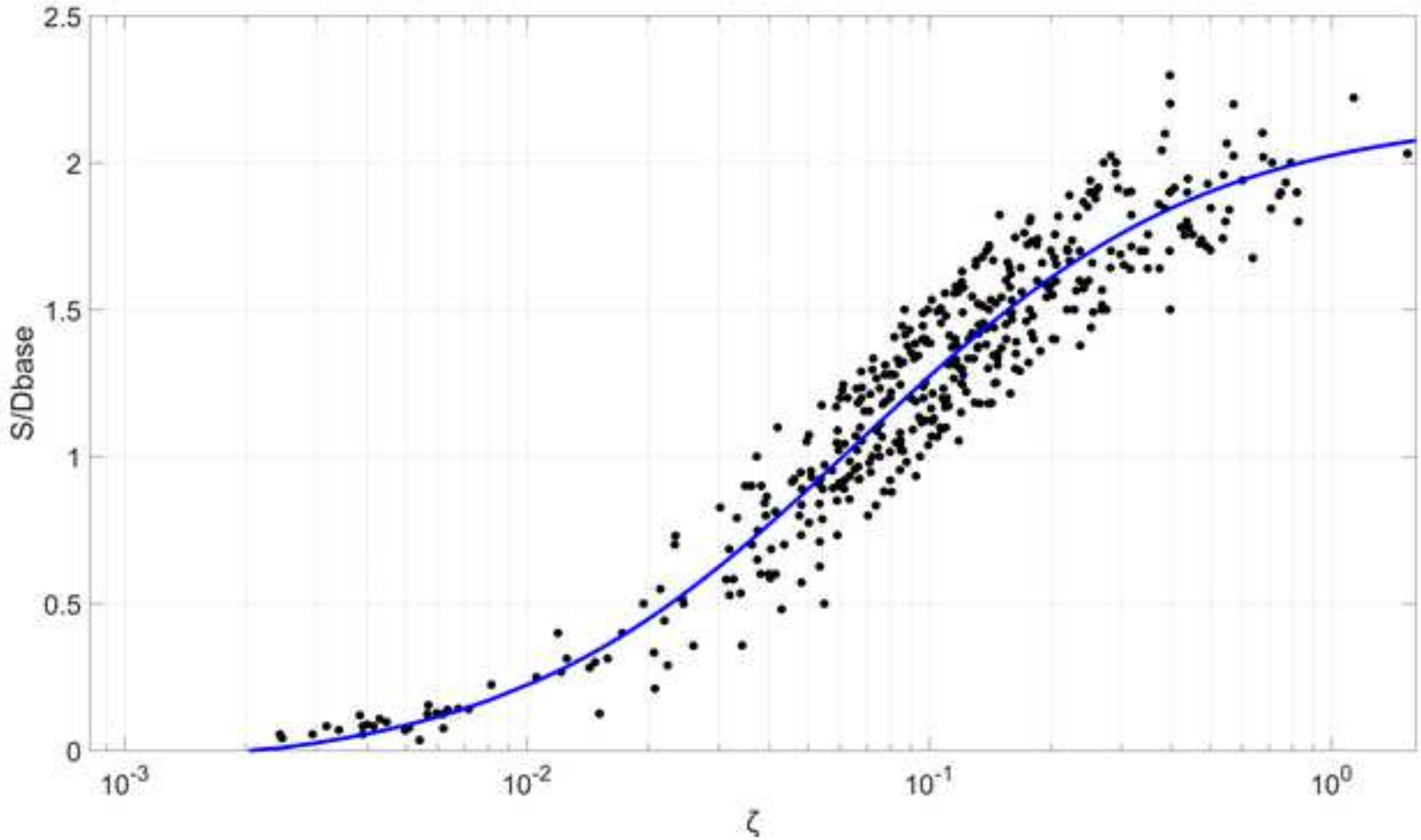

Fig. 9: Agreement of scour depth prediction (using equation 19) and measured scour depths with 10% and 20% confidence bounds.

Click here to download Figure Fig. 9.tif

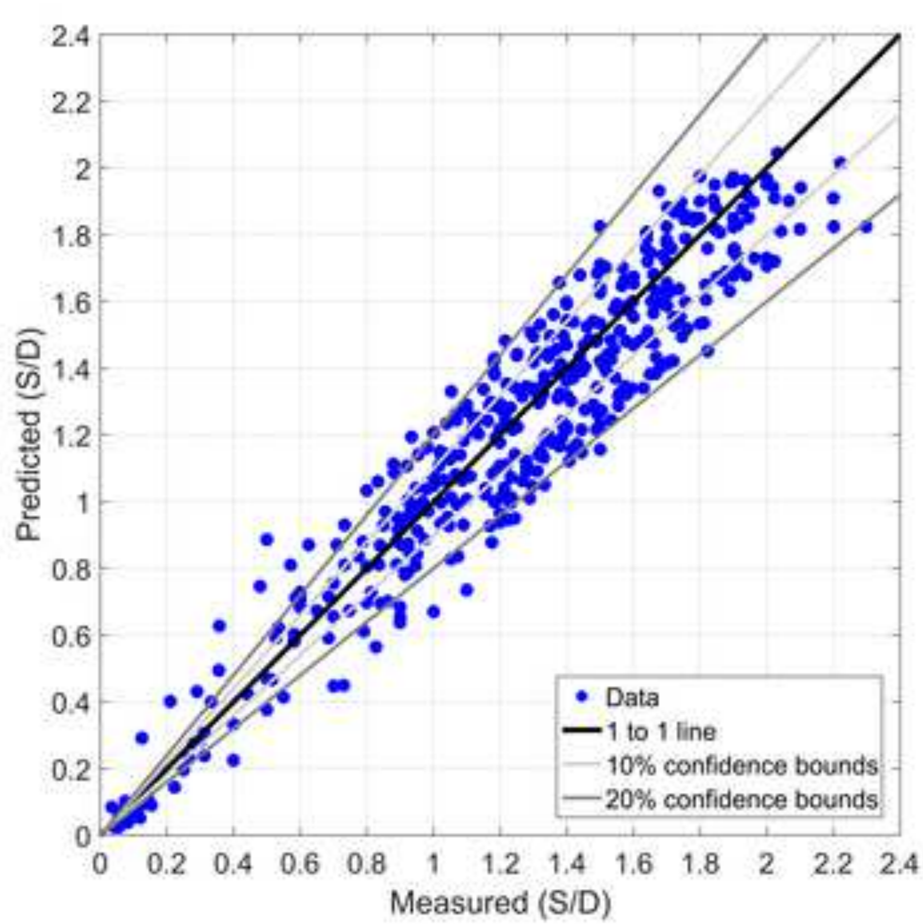

Fig. 10. Influence of the sediment mobility ratio (U/U_c={0.74.0.88 and 1}) on the variation of the equilibrium scour depth as a function of ⟨Eu⟩. Solid line shows the

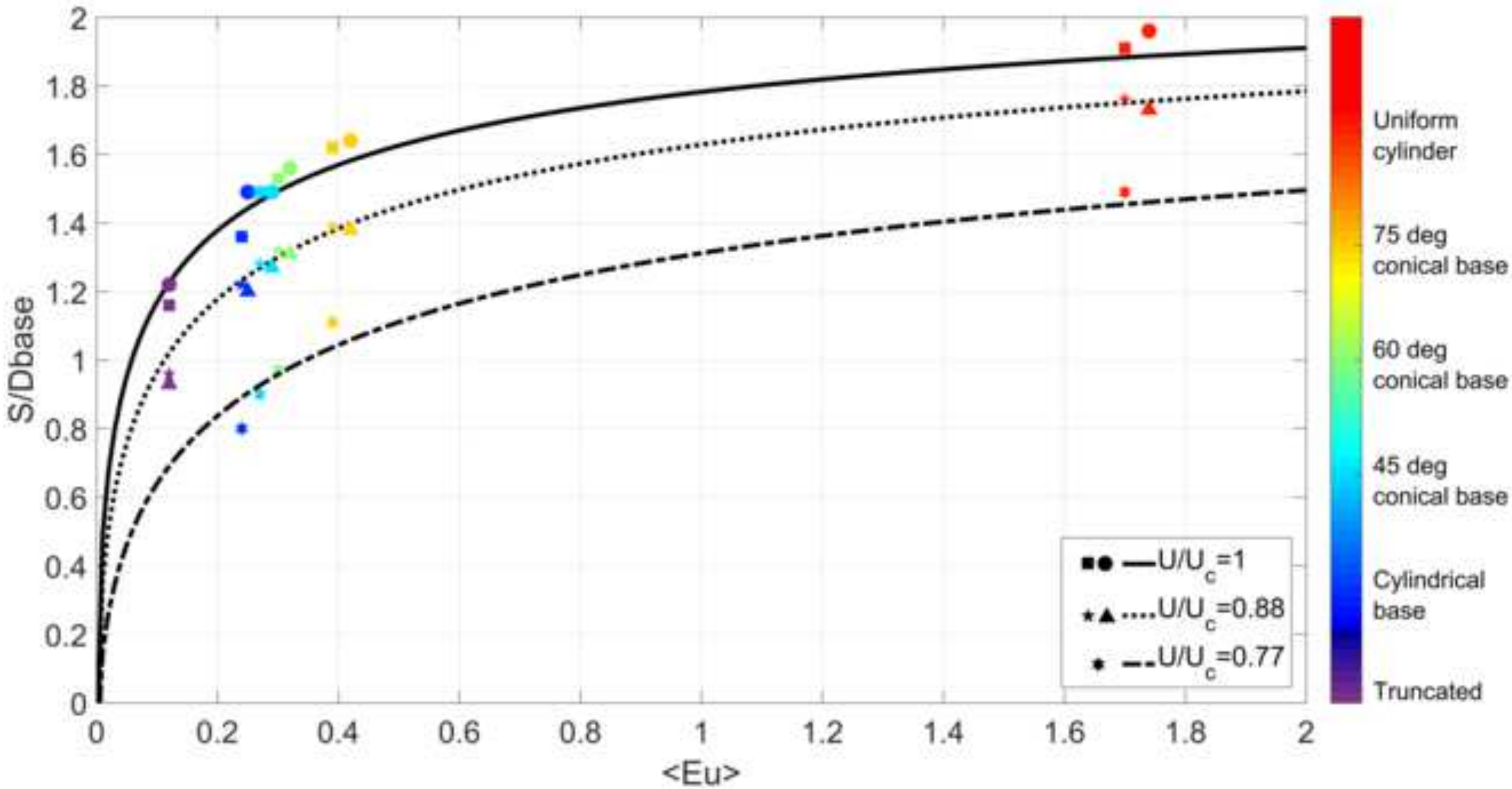

Fig. 11. Influence of the non-dimensional water depth (h/D={2.2 and 3.7}) on the variation of the equilibrium scour depth as a function of ⟨Eu⟩. Solid line shows the

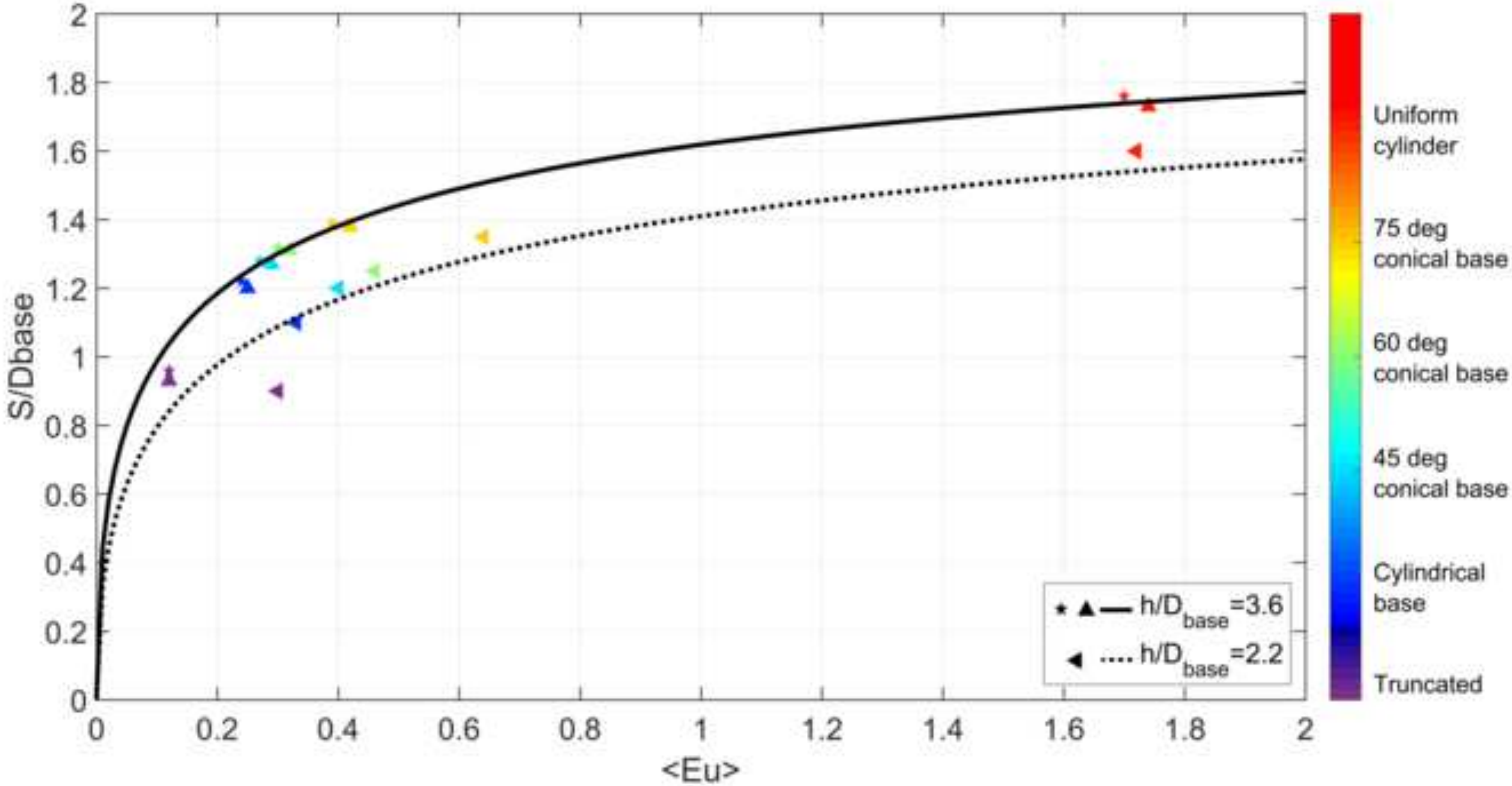

Fig. 12. Influence of the vertical flow distribution on the variation of the equilibrium scour depth as a function of ⟨Eu⟩. Solid line shows the prediction given be equation 19

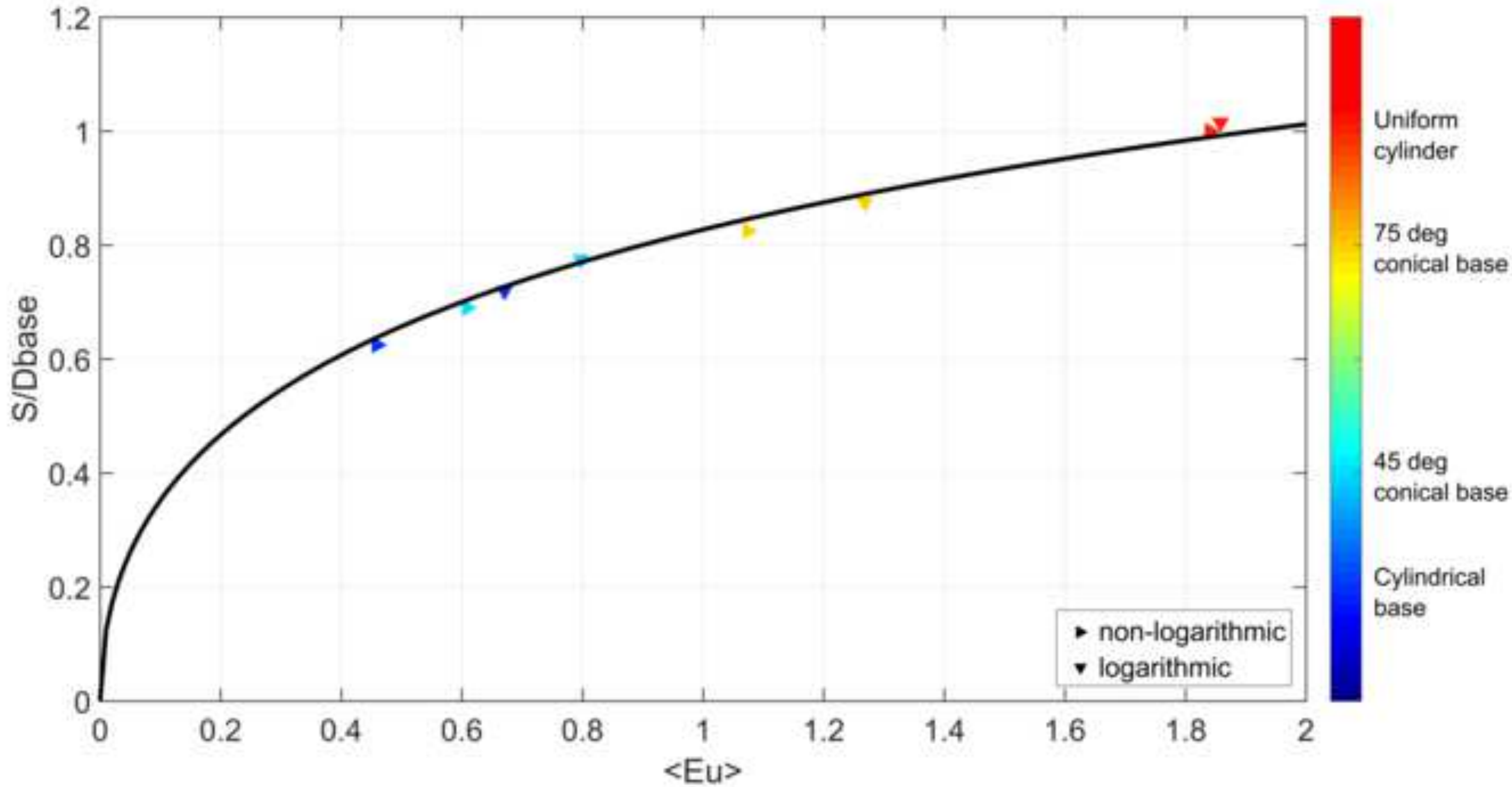

Fig. 13. Influence of 〖Re〗_D on equilibrium scour. Comparison of equation (19) to scour depth data with varying 〖Re〗_D and Fr={0.15-0.20},U/U_c ={0.7-0.85},h/D={2-

Click here to download Figure Fig. 13.tif

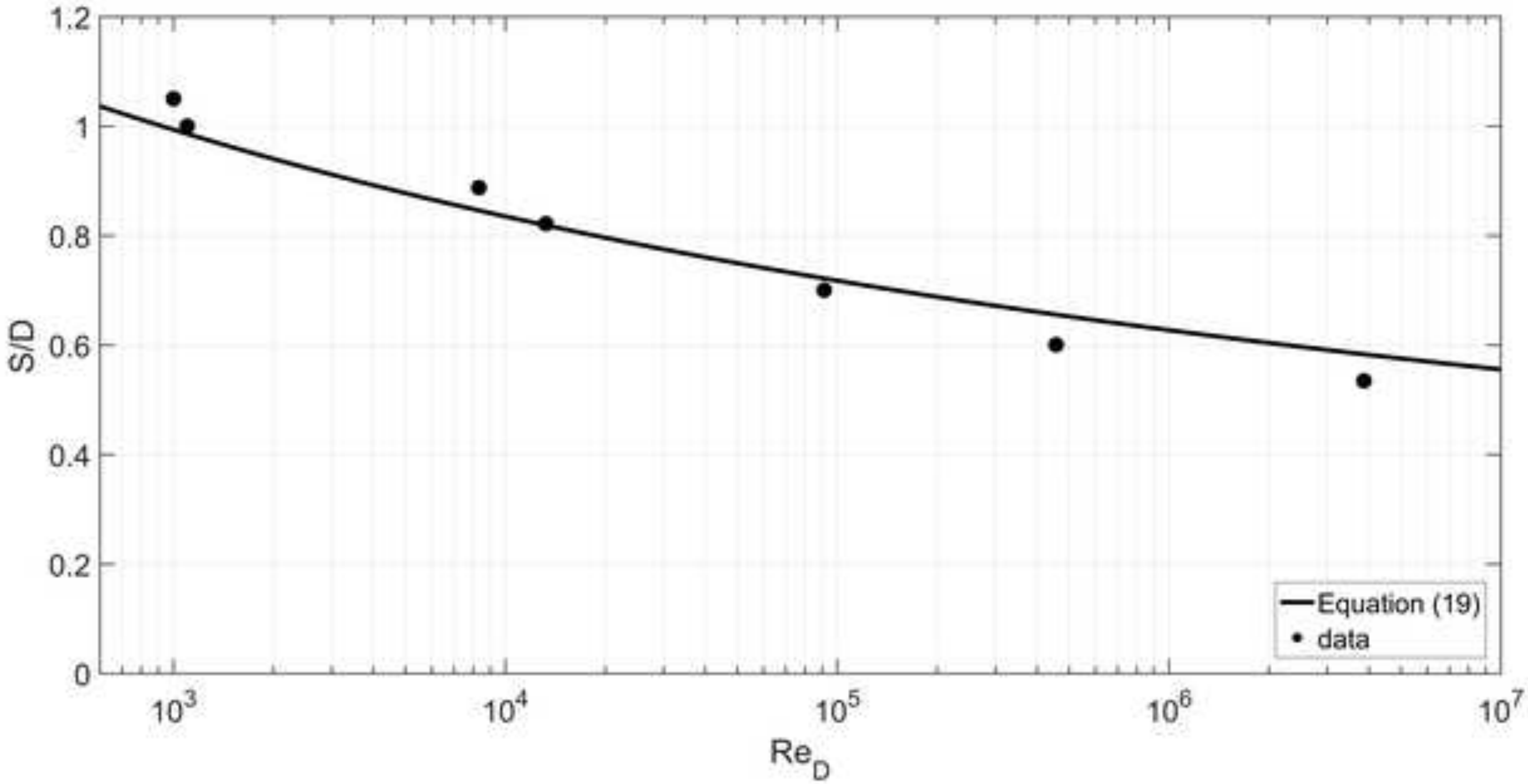

Fig. 14. Effect of the pile Reynolds number on scour. Comparison of present equation (eq. 19) and the equation of Shen et al, (1969) (eq. 21) to the data presented in

Click here to download Figure Fig. 14.tif

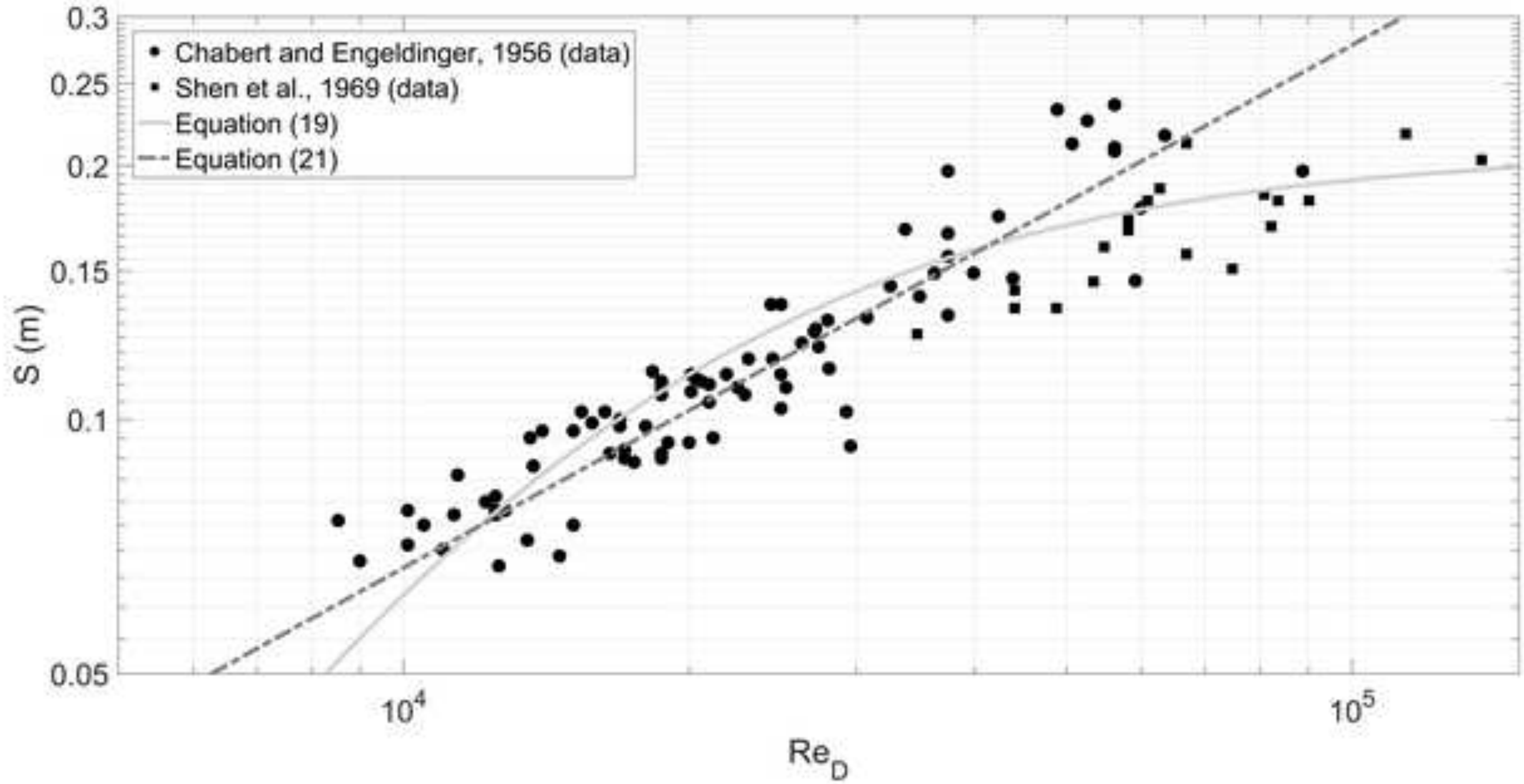

Fig. 15. Definition diagram of the location of the vertical stagnation point.

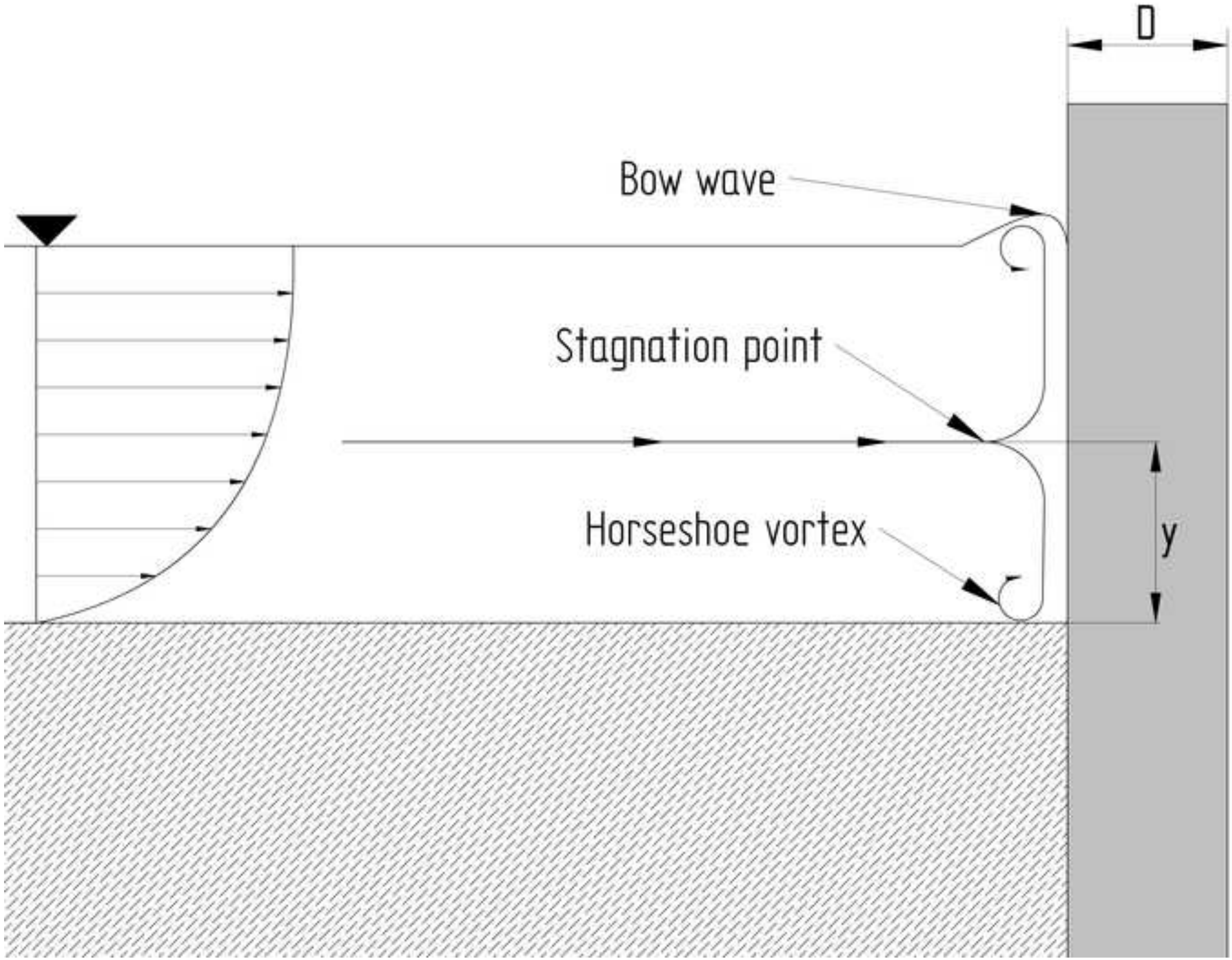

Fig. 16. Influence of Fr on equilibrium scour. Comparison of equation (19) to scour depth data with varying Fr and 〖Re〗_D={75000-150000},U/U_c ={0.8-1},h/D={2-3}

Click here to download Figure Fig. 16.tif

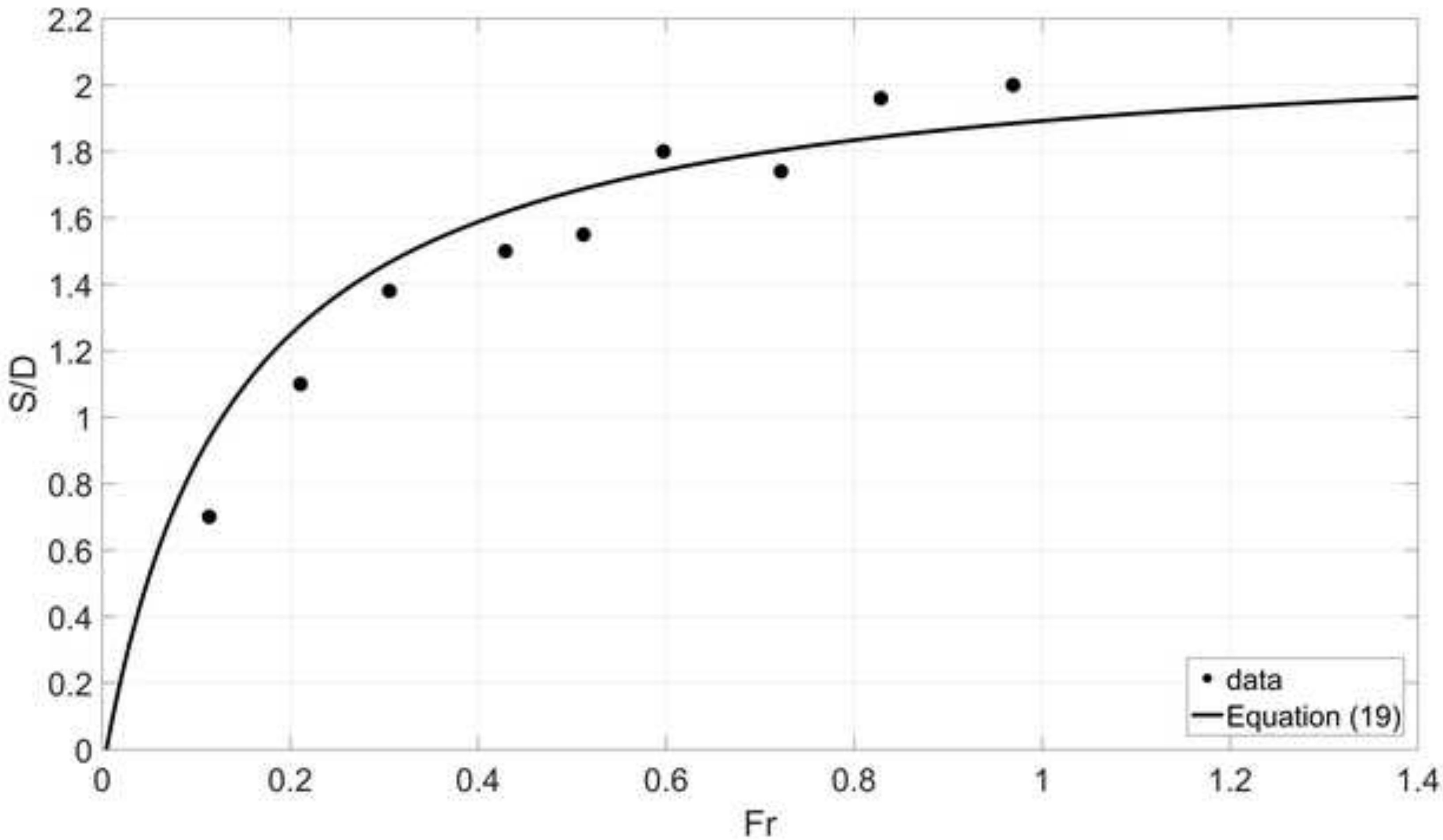

Fig. 17. Influence of h/D on equilibrium scour. Comparison of equation (19) to scour depth data with varying h/D and 〖Re〗_D={100000-300000}, U/Uc={0.8-1}, Fr={0.1-

Click here to download Figure Fig. 17.tif

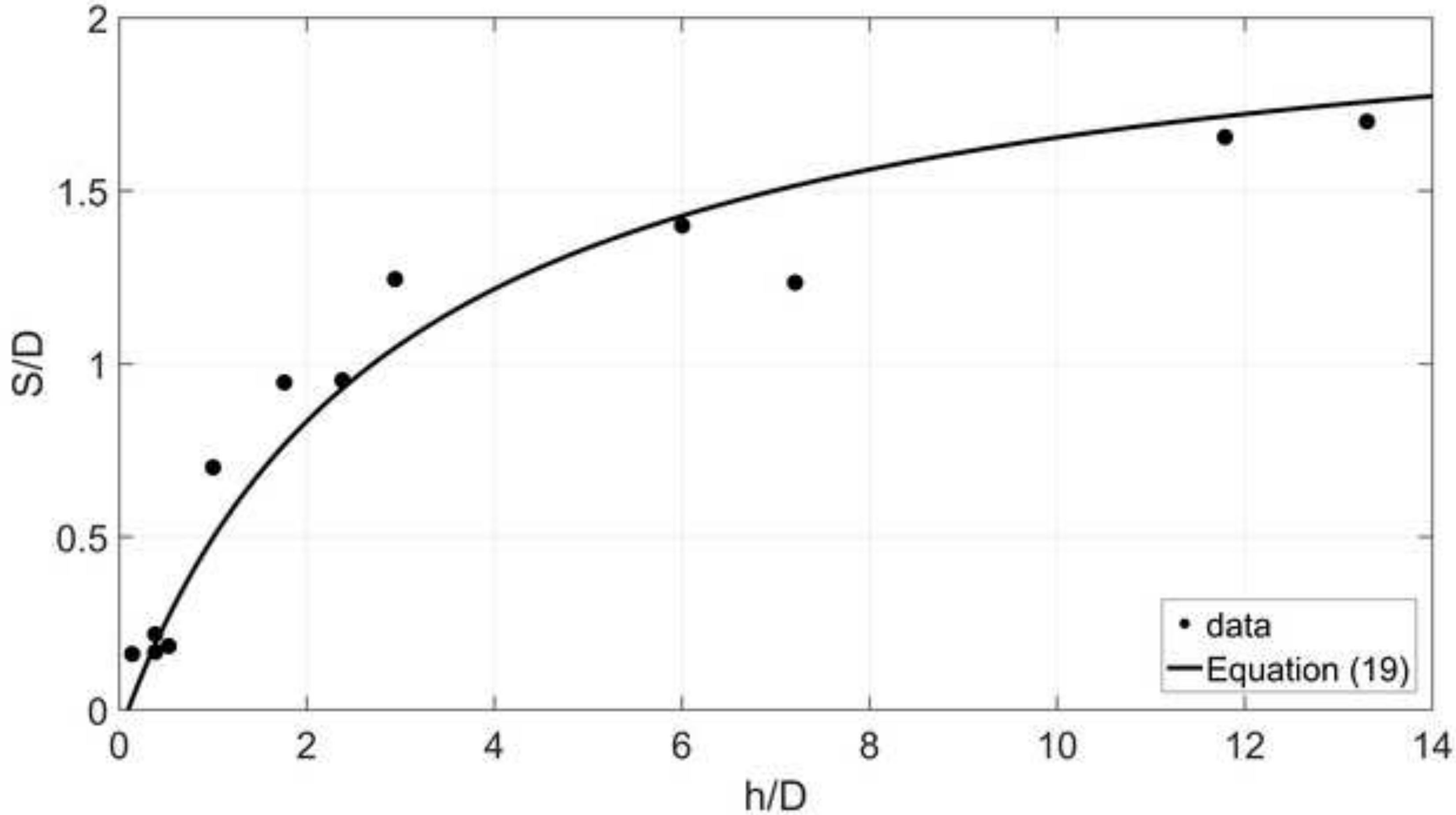

Fig. 18. Effect of boundary layer thickness on scour. Comparison of equation (19) with clearwater scour data compiled from Melville and Sutherland (1988).

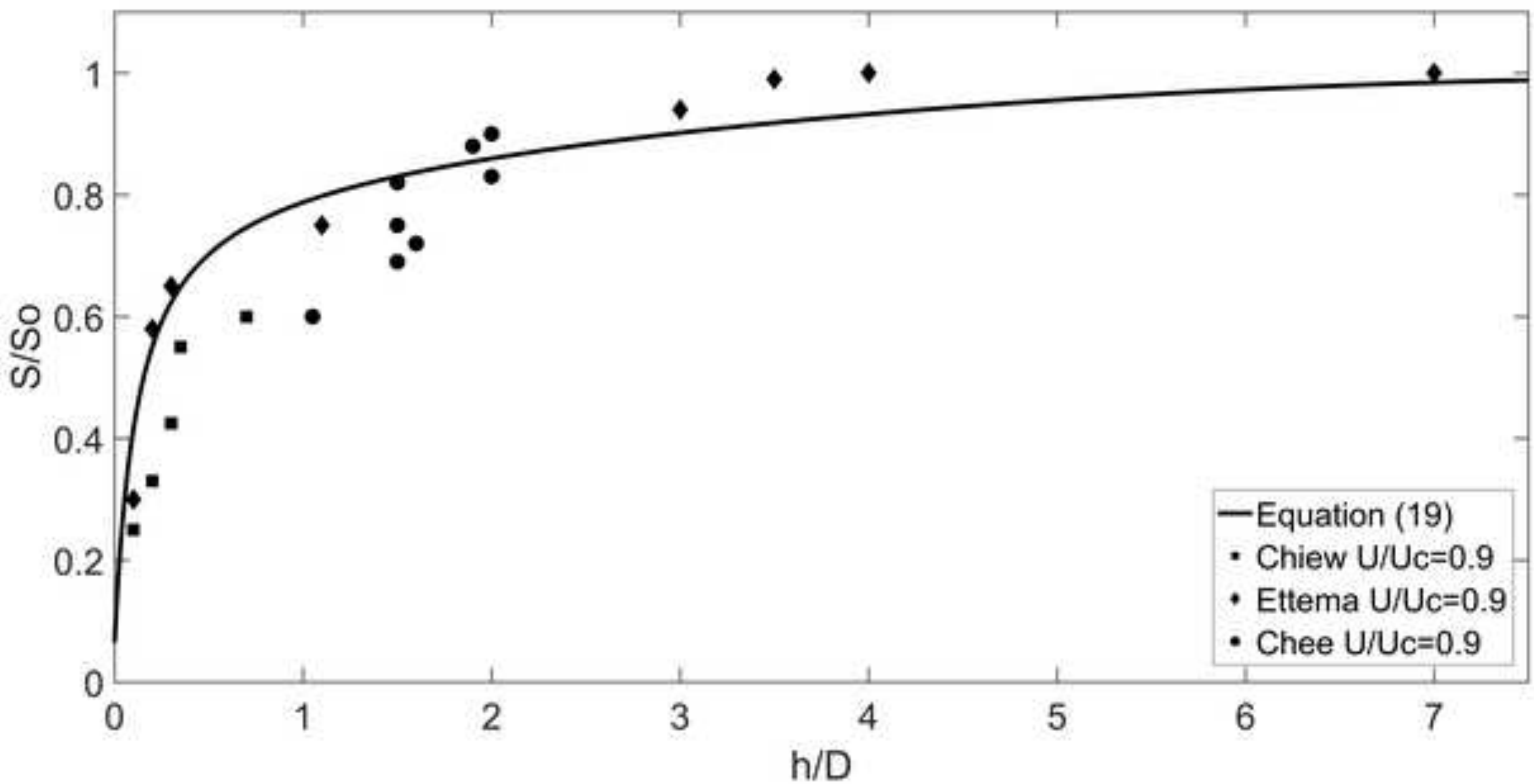

Fig. 19. Effect of sediment mobility ratio on scour for monopiles. Comparison of equation (19) to scour depth data with varying U/U_c and 〖Re〗_D={50000-